DNA Double-Strand Break Movement in Heterochromatin Depends on the *Drosophila* Histone Acetyltransferase Gcn5.

Apfrida Kendek[1, *], Arianna Sandron[1, *], Jan-Paul Lambooij[1], Serafin U. Colmenares[2], Paula Sobrevals Alcaraz[1], Robert van Es[1], Severina M. Pociunaite[1], Iris Gooijers[1], Lars de Groot[1], Gary H. Karpen[2, 3] and Aniek Janssen[1, 4]

[1] Center for Molecular Medicine, University Medical Center Utrecht, Universiteitsweg 100, 3584 CG, Utrecht, the Netherlands

[2] Department of Molecular and Cell Biology, University of California Berkeley, Berkeley, USA

[3] Division of Biological Sciences and the Environment, Lawrence Berkeley National Laboratory, Berkeley, USA

[4] Correspondence to: a.janssen-2@umcutrecht.nl

[*] These authors contributed equally

Abstract

Cells employ diverse strategies to repair double-strand breaks (DSBs), a dangerous form of DNA damage that threatens genome integrity. Eukaryotic nuclei consist of different chromatin environments, each displaying distinct molecular and biophysical properties that can significantly influence the DSB repair process. Specifically, DSBs arising in the compact and silenced heterochromatin domains have been found to move to the heterochromatin periphery in mouse and *Drosophila* to prevent aberrant recombination events. However, it is poorly understood how chromatin components, such as histone post-translational modifications, contribute to these DSB movements within heterochromatin. Using cultured cells and an *in vivo* single-DSB system in *Drosophila*, we identify that histone H3 lysine 9 acetylation (H3K9ac) is enriched at DSBs in heterochromatin but not euchromatin. We find that this enrichment is mediated by the histone acetyltransferase Gcn5, which rapidly localizes to heterochromatic DSBs. Moreover, we demonstrate that in the absence of Gcn5, heterochromatic DSBs display impaired recruitment of the SUMO E3 ligase Nse2/Qjt and fail to relocate to the heterochromatin periphery to complete repair. In summary, our results reveal a previously unidentified role for Gcn5 and H3K9ac in heterochromatin DSB repair and underscore the importance of differential chromatin responses at hetero- and eu-chromatic DSBs to promote safe repair.

Introduction

DNA Double-Strand Breaks (DSBs), in which both strands of the DNA helix are severed, are one of the most harmful lesions known to occur in genomes. DSBs can be caused by both exogenous and endogenous sources, and when repaired improperly can directly result in the formation of aberrant chromosome structures linked to genetic diseases and cancer[1–4]. The two main DSB repair pathways in eukaryotic cells are Homologous Recombination (HR) and Non-Homologous End-Joining (NHEJ). HR requires 5' to 3' end-resection at the DSB site, which results in a single-stranded 3' DNA end that invades and perfectly copies

a homologous sequence to safely repair the DSB. In contrast, NHEJ involves simple ligation of the DSB, but often results in small nucleotide insertions or deletions at the repaired site[5,6].

How different chromatin environments influence the cellular response to DSBs is less well understood[7]. Eukaryotic nuclei can be roughly subdivided into two types of chromatin: euchromatin, which has a more open conformation and contains most of the transcriptionally active protein-coding genes, and heterochromatin, which is more compact and relatively gene poor. Constitutive heterochromatin is one of the most prominent types of heterochromatin and is localized at peri-centromeric and sub-telomeric regions. It contains highly repetitive DNA sequences, which are enriched for Histone H3 Lysine 9 di- and tri-methylation (H3K9me2/3) and its epigenetic reader protein Heterochromatin Protein 1a (HP1a in *Drosophila*, HP1α in mammals)[8–13]. Moreover, constitutive heterochromatin often coalesces into one or a few cytologically distinct domains in interphase nuclei[14,15], which represent biocondensates that form through the distinct biophysical properties of HP1a[16,17].

The highly repetitive sequence content within this compact domain makes constitutive heterochromatin especially vulnerable to erroneous recombination events between homologous sequences present on non-homologous chromosomes. Previous work in *Drosophila* and mouse has revealed that heterochromatic DSBs can undergo end-resection within the heterochromatin domain, but only complete HR once relocated to the heterochromatin- or nuclear-periphery[18–21]. This DSB movement is thought to prevent aberrant HR repair within the repeat-rich heterochromatin domain[18,22].

Several proteins have been found to be rapidly recruited to heterochromatic DSBs and promote DSB movement and HR repair. These include the structural maintenance of chromosomes 5/6 (SMC5/6) complex and the associated SUMO E3 ligases/Nse2 homologs, Cervantes (Cerv) and Quijote (Qjt)[18,19,23]. SMC5/6, as well as the other two SMC complexes cohesin and condensin, are conserved throughout the kingdoms of life[24]. The characteristic ring shape of SMC complexes enables them to bring multiple DNA sequences into close proximity and thereby play a crucial role in genome folding and organization[24–26]. SMC5/6 is known to promote genome stability in various pathways including chromosome segregation [27,28], telomere maintenance[29] and DNA damage repair[30–33]. More specifically, the recruitment of SMC5/6 and its SUMO E3 ligase subunit Nse2 to heterochromatic DSBs in *Drosophila* is thought to mediate the SUMOylation of target proteins and in turn facilitate heterochromatic DSB movement through downstream signaling cascades[19,23].

Although many histone modifications have been identified at euchromatic DSB sites[34,35], histone changes at heterochromatic DSBs remain poorly understood. However, the distinct molecular and biophysical properties of heterochromatin suggest that DSB repair in this compact region requires specialized chromatin changes to allow DSB movement and repair protein recruitment. In line with this, we previously identified a role for the histone demethylase *Drosophila* KDM4A (dKDM4A) in specifically promoting the demethylation of H3K9me2/3 and H3K56me2/3 at heterochromatic DSB sites, thereby supporting DSB movement and repair pathway choice within heterochromatin[36,37]. Whether this demethylation is accompanied by additional changes in heterochromatin composition remains untested.

In budding yeast and mammalian cells, the acetylation of histone H3 Lysine 9 (H3K9ac) by the histone acetyltransferase General Control Non-repressed protein 5 (GCN5) has been described to be involved in several types of DNA damage repair such as UV-damage[38], oxidative damage[39], and DSBs[40,41]. While one study reported a decrease[39], the other studies revealed increases in H3K9ac levels in cells following damage induction[38,40,41]. These studies did not distinguish the responses in different pre-existing chromatin

environments. It thus remains to be tested whether different chromatin environments, in particular the dense constitutive heterochromatin domain, differentially depend on H3K9ac for repair of damaged sites.

Using irradiation of cells in culture, as well as our previously established *in vivo* single-DSB (DR-*white*) system in *Drosophila* tissues[20], we here identify a specific increase in H3K9ac at heterochromatic DSBs. This H3K9ac is dependent on the histone acetyl transferase Gcn5, which is rapidly recruited to DSBs within the heterochromatin domain. Moreover, loss of Gcn5 results in defective DSB movement, as well as impaired recruitment of the SUMO E3 ligase Nse2/Qjt to heterochromatic DSBs. Together, our results identify a previously unrecognized role for Gcn5 and H3K9ac in the movement and repair of DSBs within the compact heterochromatin domain.

Results

The histone acetyl transferase Gcn5 deposits new H3K9ac marks at heterochromatic Double-Strand Breaks (DSBs).

In order to gain insights into the influence of chromatin factors on the process of DSB repair in heterochromatin, we sought to determine changes in chromatin composition associated with heterochromatic DSBs. We previously observed demethylation of histone H3 Lysine 9 di- and tri-methylation at heterochromatic DSBs [37]. Since demethylation is chemically required to allow other types of epigenetic modifications, we hypothesized that demethylation could lead to acetylation of Histone H3 Lysine 9 (H3K9ac). To test this, we employed our previously established DR-*white* single DSB system in *Drosophila* (**Fig. 1A**)[20]. In this system, the DR-*white* construct is integrated in a single euchromatic or heterochromatic locus in the fly genome and contains an 18 base-pair recognition sequence targeted for DSB induction by the I-SceI endonuclease. To induce the expression of I-SceI and the consequent formation of DSBs, we heat-shocked third instar larvae containing eu- or hetero-chromatic DR-*white* insertions as well as a heat-shock inducible I-SceI (hsp.I-SceI) transgene. ChIP-qPCR (Chromatin Immuno-precipitation (ChIP) followed by quantitative PCR (qPCR)) was performed on chromatin extracts upon I-SceI-dependent DSB induction (**Fig. 1B**). Interestingly, we observed that the levels of the histone mark Histone H3 Lysine 9 acetylation (H3K9ac) increased at DSBs in three of the five heterochromatic DR-*white* lines (1.6 - 2.8-fold increase), whereas H3K9ac levels decreased or remained unchanged at three euchromatic insertion sites (**Fig. 1C, S1A**). Importantly, internal controls demonstrate that the antibodies used in these experiments selectively bind H3K9ac nucleosomes (**Fig. S1B, C**).

Previous work by others in mammalian cells as well as budding yeast have reported both the accumulation and the reduction of H3K9ac levels at DNA damage sites[38–41]. However, our ChIP-qPCR results indicate that increases in this histone mark are specific to DSBs in heterochromatin. This suggests that H3K9ac is differentially regulated in response to DSBs depending on the pre-existing chromatin domain.

It has been reported that H3K9ac deposition in *Drosophila* mainly depends on the histone acetyl transferase (HAT) Gcn5 and to a lesser extent on Elp3[42–45]. To assess which of these two HATs could be responsible for the acetylation of lysine 9 on histone H3 in *Drosophila*, we knocked down both proteins via RNA interference in *Drosophila* cells (**Fig. S1D, E**), followed by immunofluorescence staining for H3K9ac. We find that depletion of Gcn5, but not Elp3, leads to decreased nuclear H3K9ac levels in undamaged cells, supporting the notion that Gcn5 represents the major acetyltransferase for H3K9ac in *Drosophila* (**Fig. S1F, G**)[46].

Next, to test whether Gcn5 or Elp3 are recruited to heterochromatic DSBs, we fluorescently tagged these proteins in *Drosophila* cells in culture. We combined their expression with fluorescently tagged HP1a (Heterochromatin Protein 1a, to visualize heterochromatin) and Mu2 (DSB protein that binds to phosphorylated H2Av (γH2Av), MDC1 homolog). Strikingly, we observed co-localization of Gcn5 with DSBs (Mu2) in the HP1a domain within five minutes following 5Gy irradiation (**Fig. 1D**), indicating that this HAT can be directly recruited to DSBs within heterochromatin. Consistent with previous observations, Elp3 localizes to the cytoplasm in undamaged cells[47], and this pattern was not affected by the induction of DSBs via ionizing radiation (5Gy) (**Fig. S1H**). Together, this suggests that Gcn5, but not Elp3, localizes to heterochromatic DSBs and represents the main H3K9ac transferase in *Drosophila* cells. We therefore focused our subsequent analyses on the potential role of Gcn5 at heterochromatic DSBs.

The observed localization of Gcn5 to DSBs in heterochromatin, and the general role for Gcn5 in H3K9ac[42] (**Fig. S1F, G**), led us to hypothesize that Gcn5 could be responsible for the observed increase in H3K9ac levels at heterochromatic DSBs (**Fig.1C**). Thus, we irradiated control and Gcn5-depleted cells and quantified the H3K9ac intensity levels in euchromatin (H3K9me3 – low) and heterochromatin (H3K9me3 - high) (**Fig. S1I**) five minutes after damage induction. In order to focus solely on DSB-dependent changes in chromatin composition, quantification was performed only on cells displaying at least one γH2Av focus (phosphorylated H2Av, used as a DSB marker) in the heterochromatin domain (**Fig. S1I, Fig. 1E**). Our results reveal a significant increase in heterochromatic H3K9ac levels after irradiation of cells in culture (**Fig. 1E**). In contrast, the H3K9ac increase was more modest and not significant in damaged euchromatic regions (**Fig. 1F**). This result recapitulates the heterochromatin-specific increase of H3K9ac levels observed using ChIP-qPCR at single DSBs *in vivo* (**Fig. 1C**), further supporting the idea that H3K9ac levels are differentially regulated in damaged euchromatin and heterochromatin. Importantly, depletion of Gcn5 abolished the damage-dependent increase in H3K9ac levels, suggesting that Gcn5 is required for the deposition of new H3K9ac marks at the sites of heterochromatic DSBs (**Fig. S1I, Fig. 1E, F**). We conclude that the histone acetyl transferase Gcn5 is responsible for depositing new H3K9ac marks at damage sites in heterochromatin upon DSB induction.

Gcn5 promotes timely movement and repair of heterochromatic DSBs.

In *Drosophila*, heterochromatic DSBs relocate to the heterochromatin- and nuclear-periphery within thirty minutes after irradiation[18–20]. Since we observed a heterochromatin-specific increase in Gcn5-mediated H3K9 acetylation as early as five minutes after irradiation (**Fig. 1D-F**), we hypothesized that this local post-translational modification is one of the factors that promote heterochromatic DSB movement. To test this, we depleted Gcn5 in *Drosophila* cells in culture and assessed the presence of DSBs (γH2Av foci) in heterochromatin (DAPI bright[18,48]) and euchromatin (DAPI weak) at specific time points following 5Gy irradiation (**Fig. 2A**). Consistent with earlier findings[18], we find in control cells that the number of heterochromatic DSBs peaked 10-20 minutes after irradiation (**Fig. 2B**, black line). This peak was followed by a steep decrease in the number of γH2Av foci located within heterochromatin, indicative of DSB movement (**Fig. 2B**)[18]. Cells depleted of Gcn5 acquired the same number of heterochromatic DSBs within a similar timeframe as control cells (**Fig. 2B**, dashed blue line). However, the number of DSBs remained high within the heterochromatin domain (30' - 180') and did not decline as steeply as in control cells (**Fig. 2A, B**). These results suggest that loss of Gcn5 results in delayed heterochromatic DSB movement when compared to the control. Additionally, in euchromatin (DAPI weak) we did not observe any differences in number of DSBs between control and Gcn5 RNAi cells (**Fig. 2A, C**). Previous studies found that Gcn5

interacts with components of the SWI/SNF complex in yeast and human cells to promote efficient H2A(X) phosphorylation at DSB sites[40,49]. In our system, we therefore expected to find a lower average number of γH2Av foci in DAPI weak[48] (which represent ~70% of the nuclei area, **Fig. 2A**) upon Gcn5 knockdown. However, we do not observe any differences in euchromatic γH2Av accumulation in control versus Gcn5-depleted cells, suggesting that either the remaining Gcn5 expression (**Fig. S1D**) is sufficient to fulfill the role in H2Av phosphorylation or perhaps a yet unknown mechanism can take over this role in *Drosophila*. Altogether, our data indicate that knockdown of Gcn5 specifically results in impaired heterochromatic DSB movement.

In previous studies, it was found that heterochromatic DSB movement is predominantly associated with repair by HR[18,21]. Early HR steps (e.g. end-resection) occur within heterochromatin, whereas the later steps of HR (i.e. Rad51 assembly) resume only after DSBs have moved outside of the heterochromatin domain [18]. Since our data reveal a delayed heterochromatic DSB movement upon Gcn5 knockdown (**Fig. 2A, B**), we wished to address whether the early HR process within the heterochromatin domain is affected in the absence of Gcn5. ATR Interacting Protein (ATRIP) is one of the proteins involved in early HR repair by binding to the RPA-ssDNA complex[50] and has been found to be efficiently recruited to both eu- and heterochromatic DSBs[18,50]. We performed live imaging of fluorescently tagged ATRIP within the heterochromatin domain (visualized with HP1a) following 5Gy irradiation in the absence and presence of Gcn5. By following ATRIP foci kinetics (time from appearance to disappearance) as well as its dynamics (movement) in the HP1a domain, we find that, in the absence of Gcn5, ATRIP foci in the HP1a domain display defective movement (**Fig. 3A-C**). In the control situation, ATRIP foci remained on average sixteen minutes in the HP1a domain (**Fig. 3C**), after which they either move (52%, **Fig. S2A**) or get resolved. In contrast, ATRIP foci in Gcn5 depleted cells remained twice as long inside the HP1a domain (on average forty-one minutes) before they moved out (32%, **Fig. S2A**) or resolve (**Fig. 3A-C**). This result is consistent with the observed retention of γH2Av foci within DAPI bright in irradiated fixed cells (**Fig. 2A-C**).
To exclude that the observed DSB repair defects are due to changes in expression of DSB repair proteins, we performed bulk RNA-sequencing (RNA-seq) of Gcn5-depleted and control cells. These data reveal that the expression of known DSB repair proteins remained unchanged upon Gcn5 depletion (**Fig. S3A, Table S1-2**). Gcn5 knockdown also had no significant effect on the expression of cell-cycle regulated genes or cell-cycle progression based on RNA-seq data and EdU staining respectively (**Fig. S3A, B, Table S3**).
Together, these results suggest that H3K9 acetylation, mediated by Gcn5, plays a crucial role in promoting the movement and HR repair of heterochromatic DSBs. We do not find a defect in ATRIP recruitment to DSBs in heterochromatin (**Fig. S2B**), indicating that early end-resection steps can occur in the absence of Gcn5 and that specifically later steps (DSB movement and repair) are significantly delayed.

Gcn5 promotes the recruitment of the SUMO E3 ligase Qjt to heterochromatic DSBs.

Our results reveal that Gcn5 plays a role in promoting the movement of heterochromatic DSBs (**Fig. 2, 3**). We therefore sought to investigate the mechanism through which Gcn5 contributes to this process. One of the most downstream regulators of DSB movement in heterochromatin is *Drosophila* Nse2 (Cervantes/Quijote), part of the SMC5/6 complex[23]. In order to test the impact of loss of Gcn5 on *Drosophila* Nse2, we monitored the effect of Gcn5 depletion on the recruitment of Quijote (Qjt) to hetero- and eu-chromatic DSBs. We irradiated cells to induce the formation of DSBs and subsequently performed live imaging of fluorescently tagged Qjt and HP1a (**Fig. 4A-C**). In line with previous studies[19,23], we find that

Qjt overlaps with the complete heterochromatin domain (defined by HP1a) in non-irradiated cells, and that Qjt foci form in both eu- and hetero-chromatin upon irradiation (**Fig. 4A-C**). These previous studies also showed that Qjt foci remain in the damaged heterochromatic domain until ~10 minutes after DSB induction, after which they move outside of the domain[19,23]. Interestingly, although we did not observe any difference in the appearance of γH2Av foci in heterochromatin 10 minutes after irradiation (**Fig. 2B**), we do find that Gcn5-depleted cells display a decreased number of Qjt foci inside the HP1a domain when compared to the control (**Fig. 4B**). Importantly, this phenotype was specific for Qjt recruitment to heterochromatic DSBs, as we observed no difference in the number of Qjt foci within euchromatin upon Gcn5 depletion (**Fig. 4C**). This result suggests that Gcn5 promotes the recruitment of Qjt to heterochromatic DSBs, which is subsequently required to guarantee the efficient and timely DSB movement outside the HP1a domain.

In order to perform a more unbiased analysis of repair factors potentially involved in the Gcn5-mediated H3K9 acetylation at DSB sites, we determined H3K9ac-protein interactors through mass spectrometry-based analysis using recombinant H3K9ac- and H3K9me3-decorated mono-nucleosomes as bait. Biotinylated nucleosomes were incubated with nuclear extracts from irradiated Kc cells to determine H3K9ac- and H3K9me3- specific binders (**Fig. S4**). Within the H3K9ac interactome, we searched for previously described heterochromatic DSB repair proteins and identified a slight enrichment for the SMC5/6 complex compared to H3K9me3. Albeit mild, the enrichment of the SMC5/6 complex in the H3K9ac interactome is in line with the reduced Nse2 (Qjt) localization at heterochromatic DSBs (**Fig. 4A, B**) and could explain Qjt's dependency on Gcn5 for heterochromatic DSB recruitment.
Altogether, the DSB movement defects (**Fig. 2, 3**) and the impaired Qjt recruitment in Gcn5-depleted cells (**Fig. 4**) suggest that Gcn5, and the Gcn5-dependent increase in H3K9ac at heterochromatic DSBs, acts as a key player in the DSB movement pathway in heterochromatin by stimulating the recruitment of crucial regulatory factors, such as the SMC5/6-Nse2 complex, to the damaged heterochromatin domain.

Gcn5 mutant flies depend on ATR for their survival.

To assess the relevance of Gcn5-mediated H3K9 acetylation in living animals, we performed a synthetic lethality assay using Gcn5 heterozygous mutant flies that contain a premature stop codon on residue 333 (Gcn5[E333st]/+) (**Fig. 5A**)[44]. Gcn5 mutant flies are homozygous lethal but are heterozygous viable[44]. We find a seventy percent reduction in Gcn5 mRNA and a significant decrease in H3K9ac levels in heterozygous mutant larvae (**Fig. 5B-D**)[44,51].
The DNA damage repair kinase Ataxia telangiectasia and Rad3 related (ATR) is one of the proteins that rapidly respond to DSB events[52]. Moreover, it has been shown to promote heterochromatic DSB movement[18]. Combining Gcn5[E333st]/+ with an ATR truncation mutation (mei41[29D])[53] results in a 30% decreased viability (**Fig. 5E**), highlighting the synergistic roles of Gcn5 and ATR in DSB repair. Altogether, these results suggest that Gcn5 mutant synthetic lethality with ATR is due to compromised heterochromatic DSB movement and repair. We propose a model in which Gcn5 mediates the local acetylation of heterochromatic H3K9 after DSB induction and demethylation. This acetylation indirectly promotes the recruitment of the SMC5/6-Nse2 complex, and thereby the timely movement and proper repair of heterochromatic DSBs (**Fig. 5F**).

Discussion

Euchromatin and heterochromatin display different molecular and biophysical properties that can affect various aspects of DSB repair, including repair timing, DSB movement and repair pathway choice[22,35]. While in recent years research has started to uncover the impact of chromatin components on DSB repair, much still remains to be discovered about how epigenetic changes at DSBs are orchestrated in different pre-existing chromatin environments[22,35]. Since DSBs arising in heterochromatin specifically require movement towards the heterochromatin- or nuclear-periphery to avoid aberrant recombination events[18–20], we hypothesized that this process is accompanied by unique changes in chromatin composition that ensure the efficient resolution of the damaged DNA. Here we tackled this question using our previously developed inducible single-DSB system in *Drosophila* tissues[20], as well as irradiated *Drosophila* cultured cells. These results extend our previous findings on dKDM4A-mediated demethylation events at heterochromatic DSBs[37] by revealing that timely repair of DSBs also depends on the Gcn5-dependent deposition of H3K9ac at the site of damage. In the absence of Gcn5, DSBs accumulate inside the HP1a domain and take twice as long to resolve or relocate outside heterochromatin (**Fig. 3**). The data further suggest that defective DSB movement results from inefficient recruitment of the SMC5/6 complex component Nse2/Qjt to heterochromatic DSBs. We therefore propose that the Gcn5-dependent deposition of H3K9ac at heterochromatic DSBs promotes movement of the damaged DNA by facilitating the recruitment of Qjt to the HP1a domain (**Fig. 5F**).

The finding that H3K9ac levels increase almost exclusively at heterochromatic DSB sites constitutes novel information. Indeed, previous work has reported both the accumulation and the reduction of H3K9ac at DNA damage sites in human and yeast cells[38–41]. However, our *in vivo* ChIP-qPCR (**Fig. 1C**) and cell data (**Fig. 1E-F**) reveal that deposition of new H3K9ac marks is specifically enhanced at heterochromatic DSBs, suggesting that the levels of this mark are regulated according to the chromatin context in which the DSB is induced. This finding might therefore explain the conflicting results from previous studies in cells[38–41], which focused on the general chromatin response to DSBs, without considering differences in chromatin composition prior to DSB induction. Altogether, our data reveal novel insights into the specificities of DSB repair in heterochromatin and the importance of Gcn5 therein.

Interestingly, we were also able to observe Gcn5 localizing to DSB sites in heterochromatin, in line with previous *in vitro* and cell studies which reported Gcn5 being recruited to euchromatic DSBs and UV damage sites in both yeast and humans[38,40,41,54]. The finding that Gcn5 localizes to heterochromatic DSBs and specifically promotes their movement opens up new research directions. For example, how exactly is Gcn5 recruited to heterochromatic DSBs? Previously, we uncovered that movement and repair of heterochromatic DSBs in *Drosophila* depend on demethylation of H3K9me3 and H3K56me3 by the demethylase dKDM4A[36,37]. It is therefore tempting to speculate that Gcn5 recruitment depends on dKDM4A, which would conveniently allow for control of H3K9ac deposition right after the demethylation of the same residue (**Fig. 5F**). Alternatively, Gcn5 recruitment might depend on one of the factors that have previously been described to be important for its presence at euchromatic DNA damage sites in yeast and mammals, including the E2F1 transcription factor or the MRN complex[38,40,55]. In these cases, however, another factor would have to confer specificity of the recruitment to heterochromatic DSBs.

We have shown that Gcn5 depletion leads to a decreased number of Qjt foci in damaged heterochromatin, suggesting that Gcn5 or H3K9ac promote the recruitment of Qjt to DSBs. It has been previously reported

that Qjt is recruited to heterochromatic DSBs as part of the SMC5/6 complex[18,19,23]. Since none of the *Drosophila* SMC5/6 complex components possess a bromodomain (BRD, acetyl reader) (Uniprot database), we hypothesize that the newly deposited H3K9ac marks do not act as direct binding sites for SMC5/6-Cerv/Qjt at DSBs[56]. However, one could envision a scenario in which Qjt is indirectly targeted by H3K9ac via an intermediate protein. Since one such protein likely contains a BRD, we searched for BRD-containing proteins in the H3K9ac proteome we obtained via mass spectrometry (**Fig. S4**). However, we could not identify any valid candidate, perhaps because of the weak nature of the binding between BRD-containing proteins and H3K9ac[57–59]. Interestingly, a recent study in yeast proposed that Gcn5 and the SMC5/6 complex can directly interact, raising the possibility that the localization of Qjt at heterochromatic DSBs could also directly depend on Gcn5 binding[32]. Finally, we and others observed that Qjt and the SMC5/6 complex are already enriched in heterochromatin in undamaged conditions[18] (**Fig. 4A**). While the role of the SMC5/6 complex in unperturbed heterochromatin is currently unknown, one intriguing possibility is that this localization pattern facilitates the fast recruitment of the complex to DSB sites upon deposition of new H3K9ac marks.

While the SMC5/6 complex is also enriched at euchromatic DSBs[31], we did not observe a recruitment defect of Qjt to DSBs in euchromatin upon depletion of Gcn5 (**Fig. 4C**). Thus, we speculate that Qjt binding to DSBs in eu- and hetero-chromatin is regulated through different pathways, where heterochromatic DSB recruitment of Qjt is promoted by Gcn5-mediated H3K9ac, while in euchromatin other pathways are likely involved.

Another plausible role for H3K9ac at heterochromatic DSBs is the modulation of structural or biophysical properties of the damaged domain. Gcn5 has been reported to be important to promote chromatin accessibility at sites of DSBs and DNA replication[60,61]. Moreover, H3K9ac is a histone mark associated with transcription and therefore highly enriched in euchromatin[62–64]. In the context of a condensate such as heterochromatin[16,17], acetylation has also been found to regulate the physical properties of chromatin by inhibiting phase separation[65]. Therefore, the enrichment of H3K9ac at heterochromatic DSBs could stimulate the formation of a more open (euchromatin-like) structure, in order to facilitate DSB movement, as well as the recruitment of repair factors.

Finally, the identified synthetic lethality between ATR and Gcn5 mutant flies suggest that the correct functioning of the Gcn5-mediated DSB movement pathway is important to preserve genome stability. Since both ATR[18] and Gcn5 (this study) are required for proper movement of DSBs, we suggest that the decreased viability associated with the mutations in both proteins is due to the defective repair of heterochromatic DSBs. Although we cannot exclude that the synthetic lethality is caused by the contributions of Gcn5 to the recruitment of the SWI/SNF remodeling complex[40,49], we did not observe any defect in the γH2Av accumulation and resolution in euchromatin (**Fig. 2C**), suggesting that euchromatic DSB repair can occur in the absence of Gcn5 in *Drosophila*.

Overall, our results provide an exciting illustration of how heterochromatin uniquely responds to a DSB, and modifies its chromatin features to promote successful repair. This is in line with the idea that chromatin components and chromatin-associated factors actively participate in the process of DSB repair and are fine-tuned depending on the respective chromatin domain[22,37,66]. Future research into how diverse chromatin environments affect and regulate the response to DSBs therefore represents a critical goal in

order to understand not only how genomic stability is maintained across the eukaryotic nucleus, but also how failure to maintain genomic integrity can result in disease development.

Figure Legends

Figure 1. H3K9ac is increased at heterochromatic DSBs in a Gcn5-dependent manner. A. Schematic representation of the DR-*white* system in *Drosophila*. The DR-*white* construct is integrated in a single euchromatic or heterochromatic locus in the fly genome to generate different lines (Eu_1-3 and Het_1-5). The DR-*white* construct contains an 18-basepair DNA sequence targeted by the I-SceI endonuclease, resulting in the formation of a single DSB[20]. **B**. Scheme detailing the DSB induction protocol in DR-*white* fly lines. Chromatin was extracted 6 hours after DSB induction. DSBs were induced by a 1-hour heat shock (37°C) of third instar DR-*white* larvae containing a heat-shock promoter-driven I-SceI transgene (hsp.I-SceI). To control for heat-shock effects, all conditions (without/with hsp.I-SceI) are heat shocked. **C**. ChIP-qPCR analysis of H3K9ac levels at indicated DR-*white* loci. The qPCR primers reside 1.4 kb downstream of the I-SceI cut site ("3xp3" in *Fig. 1A*). Fold change is calculated by dividing the enrichment levels of H3K9ac in the damaged (+ DSB, + I-SceI) samples by those in the control (-DSB, no I-SceI) samples. The grey dotted line represents a fold change of 1, in which H3K9ac levels are unchanged upon DSB induction. All qPCR results are relative to an internal control region (*yellow*), which is consistently enriched for H3K9ac. Error bars represent mean±SD from ≥4 independent experiments. **D**. Representative time-lapse images of non-irradiated (no IR) and irradiated (5 minutes after 5 Gy gamma-irradiation) Kc cells with fluorescently tagged Mu2 (green, DSB marker), Gcn5 (blue) and HP1a (magenta, heterochromatin marker). Arrows indicate Gcn5 localizing to a heterochromatic DSB. Scale bars = 2µm. **E, F**. Quantification of H3K9ac intensity levels in heterochromatin (*E*, H3K9me3-enriched, stainings performed as in *Fig. S1I*) and euchromatin (*F*, low H3K9me3, see *Fig. S1I*) in non-irradiated versus irradiated control (yellow dsRNA) and Gcn5-depleted Kc cells. Irradiated cells were fixed 5 minutes after damage induction. Graphs represent three independent experiments per condition. Each big circle (grey, blue, magenta) represents the average intensity within one experiment. Small circles represent individual cells within one experiment. (n.s) P-value>0.05, (*) P-value≤0.05, (**) P-value≤0.01 (***) P-value≤0.001, paired t-test (**C**) and one way ANOVA followed by Tukey's multiple comparison (**E** and **F**).

Figure 2. Gcn5 knockdown results in delayed heterochromatic DSB movement. A. Representative images of Kc cells depleted for yellow (control) and Gcn5, fixed at indicated time points following 5Gy irradiation. Cells were stained for γH2Av (green, DSB marker) and DAPI (magenta). White arrows indicate γH2Av focus in DAPI bright domain (heterochromatin). Cells at time point 0 were fixed without prior irradiation. Scale bar = 2µm. **B, C**. Quantification of images as in *A*. Average number of γH2Av foci in DAPI bright (**B**) and DAPI weak (**C**) is shown at indicated time points. Shade bars represent mean±SD of 3 independent experiments. (**) P-value ≤ 0.01, paired t-test. HET = heterochromatin, EU = euchromatin.

Figure 3. Gcn5 knockdown results in prolonged retention of ATRIP in HP1a domain. A. Representative time lapse images of ATRIP foci (green, HR protein) within the HP1a domain (magenta) in irradiated (5Gy) control (yellow dsRNA) or Gcn5 depleted Kc cells. Scale bars = 2µm. Insets are zoom-in view of the heterochromatic ATRIP foci. **B.** Quantification of time-lapse movies as in *A*. ATRIP foci movement and kinetics plotted from their appearance in the HP1a domain (0', magenta) to the timepoint they moved outside of the HP1a domain (out, grey) or resolved (disappear, black). Each row indicates quantification of one ATRIP focus**. C.** Quantification of the mean residence time of ATRIP foci within the HP1a domain. (*) P-value ≤ 0.05, paired t-test. Error bars represent mean+SD of 3 independent experiments.

Figure 4. Gcn5 knockdown leads to a decrease in Qjt recruitment at heterochromatic DSBs. A. Representative time-lapse images of Kc cells expressing HP1a (magenta, heterochromatin) and Qjt (Nse2,

green). Arrowhead indicates Qjt focus residing inside the HP1a domain. Scale bars = 2µm. **B, C**. Quantification of Qjt foci inside the HP1a domain (**B**) and in euchromatin (**C**, outside HP1a domain) in non-irradiated versus 10 min after irradiation control (yellow dsRNA) and Gcn5-depleted Kc cells. HET = heterochromatin, EU = euchromatin. Error bars represent mean+SD from three independent experiments. (n.s) P-value>0.05, (*) P-value≤0.05, (***) P-value≤0.001, one way ANOVA test followed by Tukey's multiple comparison.

Figure 5. Gcn5 mutant is synthetically lethal with ATR mutant. A. Schematic representation of Gcn5[E333st] mutation. Gcn5 consists of 3 exons (black rectangles) and 2 introns (lines in between the black rectangles). The premature stop codon (E333st, orange arrow in first exon) is introduced in the three nucleotides encoding for the 333rd amino acid[44]. **B**. Normalized expression levels of Gcn5 in control (OregonR) and Gcn5[E333st]/+ third instar larval tissues as determined by RT-qPCR. Graph represents average from three independent experiments. Error bar indicates mean+SD. **C**. Representative images of *Drosophila* wing discs dissected from L3 stage larvae of OregonR (Control) or Gcn5[E333st]/+ and immuno-stained for H3K9ac. Scale bar = 2µm. **D**. Quantification of H3K9ac intensity per cell for the wing discs depicted in *C*. Lines represent mean intensity. **E**. Synthetic lethality assay of Gcn5 mutant with ATR mutant. N=310 flies for the control line (Gcn5 mutant, wild-type ATR allele (mei41+; Gcn5[E333st]/+)) and n=344 flies for the cross between Gcn5- and ATR- mutant flies (mei41[29D]; Gcn5[E333st]/+). **F**. Model for the role of Gcn5-mediated H3K9ac in heterochromatic DSB repair. The local transfer of an acetyl group onto H3K9 by Gcn5 at heterochromatic break sites leads to recruitment of SMC5/6-Nse2 (Qjt) which in turn promotes movement and repair of heterochromatic DSBs.

Supplemental figures/tables

Figure S1. Gcn5 controls H3K9ac levels in *Drosophila.* A. ChIP-qPCR result for H3K9ac in three euchromatic and five heterochromatic DR-*white* lines, with (hsp.I-SceI) and without (no hsp.I-SceI) DSB induction. Graph indicates the percentage of input (normalized to internal *yellow* control gene) of H3K9ac from the same experiments as in *Fig. 1C*. Error bars represent mean±SD from ≥4 independent experiments. **B**, **C**. Specificity test for two anti-H3K9ac antibodies from Epicypher (*B*, lot number 13-0020, *C*, lot number 13-0033). Specificity was determined by using the SNAP-ChIP K-AcylStat nucleosome panel from Epicypher. Error bars indicate mean±SD for ≥3 independent experiments. H3 un = unmodified H3. **D, E**. Normalized expression levels of Gcn5 (*D*) and Elp3 (*E*) in control (yellow dsRNA) and HAT-depleted Kc cells, determined by Reverse Transcription followed by quantitative PCR (RT-qPCR). Graph represents mean±SD from three independent experiments. **F**. Immunofluorescence staining for H3K9ac in control, Gcn5-depleted and Elp3-depleted S2 cells. **G**. Quantification of absolute nuclear H3K9ac intensity levels in control, Gcn5-depleted and Elp3-depleted S2 cells. Each bigger circle (grey, blue, magenta) represents the average intensity within one experiment. Smaller circles represent individual cells within one experiment. **H**. Representative time-lapse images of non-irradiated and 5Gy-irradiated Kc cells of fluorescently tagged Mu2 (green, DSB marker), Elp3 (blue) and HP1a (magenta, heterochromatin marker). Images were taken 10 minutes after IR. Scale bars = 5µm. **I**. Representative immunofluorescence images for the quantification shown in *Fig. 1E, F*. Non-irradiated and irradiated control (yellow dsRNA) and Gcn5-depleted Kc cells were stained for H3K9ac (blue), H3K9me3 (magenta, heterochromatin marker) and γH2Av (green, DSB marker). Arrowheads indicate γH2Av foci within heterochromatin. For **F,** and **I**, scale bars = 2µm. For **A** and **G**, (n.s)

P-value>0.05, (*) P-value≤0.05, paired t-test (**A**) and one way ANOVA followed by Tukey's multiple comparison (**G**).

Figure S2. Gcn5 knockdown affects ATRIP foci movement. A. Quantification of the percentage of ATRIP foci that eventually move out of HP1a domain as depicted in *Fig. 3B*. **B**. Quantification of the average number of cells with ATRIP foci inside HP1a domain upon control (yellow dsRNA) or Gcn5 depletion within the window of time imaged (120 minutes). Error bars represent mean+SD of 3 independent experiments.

Figure S3. Gcn5 knockdown does not affect transcription of DSB repair genes or cell cycle stage. A. Volcano plot for bulk RNA-sequencing of Kc cells depleted of Gcn5 or yellow (control). See Table S1-3 for more details. **B**. Quantification of the percentage of EdU positive (S-phase) Kc cells upon Gcn5 and yellow (control) knockdown. Error bars represent mean+SD of 3 independent experiments.

Figure S4. Mass spectrometry identification for H3K9ac vs H3K9me3 binders upon DSB. *(top)* Schematic representation of mass spectrometry experiment. Biotinylated mono-nucleosomes containing H3K9ac and H3K9me3 were incubated for 90 minutes at room temperature with nuclear extracts from 5Gy irradiated Kc cells. *(bottom)* Volcano plot representing the H3K9ac *(left)* and H3K9me3 *(right)* interactomes. Known H3K9me3-binders are highlighted in blue.

Tables S1-3. Detailed list of significantly up- and downregulated genes (p-adj<0.05 and |log2 fold change|>0.58) (Table **S1**), repair protein genes (Table **S2**) and cell cycle regulated genes (Table **S3**) in Kc cells depleted of Gcn5 as determined by RNA-sequencing (also see volcano plot in *Fig. S3)*.

Materials and Methods

Constructs

ATRIP, Qjt, GCN5, elp3, Mu2 and HP1a were each cloned from cDNA generated from wild type adult flies. cDNA for each gene was cloned into a pCopia plasmid backbone containing an N-terminal fluorescent tag (CFP, YFP, GFP, or mCherry).

Fly lines and genetic assays

All fly lines were reared at room temperature in standard medium unless otherwise stated. DR-*white* fly lines have been previously described[20]. Heterozygous Gcn5[E333st] flies were obtained from the Bloomington *Drosophila* Stock Center (#9333) and the mei41[29D] mutant line was kindly provided by Tin Tin Su.

Chromatin Immunoprecipitation-quantitative PCR (ChIP-qPCR)

Third instar larvae from DR-*white* fly lines containing the *hsp.I-SceI* transgene were heat-shocked at 37°C for 1 hour and snap-frozen in liquid nitrogen 6 hours after heat shock treatment. Larvae from DR-*white* fly lines not containing the *hsp.I-SceI* transgene were used as a control and subjected to the same heat shock

treatment. Frozen larvae were stored at -80°C until chromatin extracts preparation. For chromatin extracts preparation, 80 larvae per line were homogenized, fixed and sonicated as described within the modENCODE project (https://www.encodeproject.org/documents/f890fde6-924c-4265-a60f-c5810401066d/, ChIP protocol by Kevin White lab)[67]. ChIP procedures were performed on chromatin extracts as previously described[68]. Each ChIP sample was prepared with 2µg of chromatin extract and 5µg of anti-H3K9ac antibody. qPCR was employed to quantify the enrichment levels of histone marks of interest using the qPCR FastStart Universal SYBR Green Master Mix (Roche) and qPCR specific primers targeting the I-SceI site (3xp3) or the *yellow* gene as a control (Table S4).

Cell culture, dsRNA production and transfection

S2 and Kc167 (Kc) cells were cultured at 27°C degrees in Schneider's Insect Medium (Sigma-Aldrich) containing 10% FBS and CCM3 Serum-Free Medium (HyClone) respectively. For RNAi experiments, dsRNA was generated by first adding a T7-promoter sequence to the region of interest via PCR, followed by reverse transcription using the MEGAScript T7 transcription kit (Life Technologies) according to the manufacturer's instructions (Table S4). 5-10µg of dsRNA was used to transfect 200.000 cells 5 days prior to irradiation. As a control, dsRNA targeting the *yellow* gene was always included. For live imaging experiments, cells were transfected with fluorescent proteins of interest approximately 6 hours prior to dsRNA transfection. For live imaging of Qjt, Kc cells were transfected with GFP-Qjt and Hygromycin resistance plasmids. Cells were selected for 2 weeks using 200µg/ml Hygromycin to generate Kc cells with stable GFP-Qjt expression. All transfections were performed using TransIT-2020 transfection reagent (Mirus) according to the supplier's manual. Irradiation was performed by exposing cells to 5Gy of γ-rays in an IBL 437C machine.

Reverse Transcription-quantitative PCR (RT-qPCR)

Knock down efficiency was verified by reverse transcription-quantitative polymerase chain reaction (RT-qPCR). To this end, cells transfected with dsRNA were harvested after 5 days and RNA was extracted using the RNeasy Micro Kit (Qiagen) according to the manufacturer's instructions. cDNA was obtained by using the iScript cDNA synthesis kit (BioRad). RT-qPCR reaction, using cDNA as template, was performed on a thermocycler using primers targeting *tubulin* as control. To test mRNA levels in Gcn5[E333st] larvae, RNA extraction and RT-qPCR were conducted as previously described[37] (see Table S4 for primers used for RT-qPCR).

Immunofluorescence (IF) and EdU staining

For IF staining on cells in culture, fixation was achieved by incubating cells with 4% Paraformaldehyde (PFA) in PBS for 5 min. Next, cells were incubated with 0.4% Triton-X diluted in PBS for 10 min to allow for permeabilization. Blocking was subsequentially performed by adding 5% milk, 0.4% Triton-X diluted in PBS for 1 h. Primary antibodies were incubated overnight at 4°C, followed by secondary antibody and DAPI incubation for 2h at RT, all diluted in blocking solution. Finally, cells were mounted on glass slides using ProLong Diamond Antifade Mountant (Invitrogen).

For IF staining of tissue, wing discs were dissected from third instar larvae in 10µl of Schneider's Insect Medium containing 10% FBS and fixed on a glass slide with 4% PFA for 5 minutes. Slides were dipped in liquid nitrogen and stored at -20°C in 99% ethanol. Slides were brought to RT, incubated in PBS for 20 min and subsequently blocked in 5% milk, 0.4% Triton-X diluted in PBS for 1.5 h. The following steps (primary and secondary antibodies incubation, mounting on glass slide) were performed as described above for fixed cells.

For EdU staining, Kc cells were incubated with 10µM EdU for 30 min. EdU detection was performed according to Click-iT EdU Imaging Kits Protocol (Invitrogen).

Antibodies and dilutions

For ChIP-qPCR, experiments were performed with the anti-H3K9ac (Epicypher 13-0020, 13-0033) antibody. For IF experiments on tissues and cells, the following primary antibodies were used: anti-H3K9ac (rabbit, Epicypher 13-0033, 1:500), anti-γH2Av (mouse, Hybridoma Bank, UNC93-5.2.1, 1:250), FlexAble Coralite Plus 555 conjugated anti-H3K9me3 (rabbit, ab8898, 1:500). The following secondary antibodies were used: Alexa goat anti-rabbit 488 (1:600), Alexa goat anti-mouse 568 (1:600) (Invitrogen).

Imaging and quantifications

Images were acquired using an RT DeltaVision microscope (DeltaVision Spectris; Applied Precision, LLC) using a 60X oil immersion objective (NA 1.40). For live imaging experiments, images were acquired every 10 minutes. Deconvolution was performed using SoftWoRx (Applied Precision, LLC) software. Image analysis was manually performed on deconvoluted images using the Fiji image analysis software.

RNA-sequencing procedure

Kc cells were depleted of Gcn5 or yellow (control) for 5 days using dsRNA as described above. Cells were harvested and RNA was isolated using the RNeasy Micro Kit (Qiagen). The quality and quantity of the RNA samples was measured using the Agilent Fragment Analyzer 5300 system and Qubit (Invitrogen) respectively. 100ng of total RNA was used to prepare TruSeq Stranded mRNA libraries (20020594) following the manufacturer's protocol with custom 384 xGen UDI-UMI adapters (IDT). Prepared libraries were validated with the Fragment Analyzer system dsDNA 910 Reagent Kit (35-1500bp) and Qubit dsDNA HS Assay Kit (Cat. Q32854). All libraries were then pooled in equimolar ratio and sequenced on a Nextseq2000 (Illumina) by using a P2 flow cell with 50bp paired-end reads.

RNA-sequencing data analysis

Quality control on the sequence reads from the raw FASTQ files was performed with FastQC (v0.11.8). TrimGalore (v0.6.5) was used to trim reads based on quality and adapter presence after which FastQC was again used to check the resulting quality. rRNA reads were filtered out using SortMeRNA (v4.3.3) followed by alignment to the reference genome fasta (Drosophila_melanogaster. BDGP6.32) using the STAR (v2.7.3a) aligner. Followup QC on the mapped (bam) files was performed using Sambamba (v0.7.0), RSeQC

(v3.0.1) and PreSeq (v2.0.3). Readcounts were then generated using the Subread FeatureCounts module (v2.0.0) with the Drosophila_melanogaster.BDGP6.32.105.chr.gtf file as annotation. CPM and RPKM Normalized versions of the counts table were generated using the R-packages edgeR (v3.28) as well as a normalized version using DEseq2 (v1.28). The differential expression analysis was performed using DESeq2.

Mass spectrometry

Biotinylated modified mononucleosomes containing either H3K9ac (16-0314) or H3K9me3 (16-0315) were purchased from Epicypher. To obtain nuclear extract from irradiated Kc cells, fourty five T75 flasks of Kc cells were grown at 27°C until confluent. Cells were then harvested, irradiated with 5Gy, kept at room temperature for 5 minutes to initiate the DSB response and then moved to 4°C until subjected to nuclear protein extraction according to established methods[69]. To extract the chromatin bound proteins we additionally used Benzonase Nuclease (EMD Millipore, 10µL/g nuclear pellet) during the extraction. The final nuclear protein extract was snap frozen in liquid nitrogen and stored at 80°C until further use.

Ten pmol of the biotinylated mononucleosomes were first coupled to 30µL Dynabeads MyOne Streptavidin T1 at 4°C for one hour in coupling buffer (200mM NaCl, 10mM Tris, 1mM EDTA, 1mM DTT and 0.1% IGEPAL). After washing with binding buffer (20mM HEPES, 150mM CH3COONa, 0.2mM EDTA, 20% glycerol, 10mM DTT, 0.1% IGEPAL), 2mg of irradiated nuclear extract diluted in binding buffer supplemented with 3mM of each ATP and GTP (NEB) were added to the streptavidin bound nucleosomes. Samples were incubated at room temperature tumbling for 90 minutes, subsequentially washed once with binding buffer and moved to new tubes. After 3 rounds of washes with binding buffer (depleted of IGEPAL), the supernatant was discarded and the streptavidin bound pellet was stored at -20°C until LC-MS/MS measurement (see Supplementary Methods for more details).

Statistics and graphs

All statistical analysis were performed in GraphPad Prism. Plots were generated in Python using Panda, Seaborn and matplotlib. Fig. 5F, chromosome icon in Fig. 1A and mass spec illustration in Fig. S4 were created with Biorender.com.

Acknowledgement

We thank the Lens and Janssen lab members for their valuable input during laboratory meetings. This work was funded by the European Research Council (ERC) under the European Union's Horizon 2020 research and innovation program, grant agreement No. 850405, and VIDI VI.Vidi.203.001 financed by the Dutch Research Council (NWO). We acknowledge the Utrecht Sequencing Facility (USEQ) for providing sequencing service and data. USEQ is subsidized by the University Medical Center Utrecht and The Netherlands X-omics Initiative (NWO project 184.034.019).

References

1. Barra, V., and Fachinetti, D. (2018). The dark side of centromeres: types, causes and consequences of structural abnormalities implicating centromeric DNA. Nat. Commun. *9*, 4340. 10.1038/s41467-018-06545-y.

2. Willis, N.A., Rass, E., and Scully, R. (2015). Deciphering the code of the cancer genome: mechanisms of chromosome rearrangement. Trends Cancer *1*, 217–230. 10.1016/j.trecan.2015.10.007.

3. Ramsden, D.A., and Nussenzweig, A. (2021). Mechanisms driving chromosomal translocations: lost in time and space. Oncogene. 10.1038/s41388-021-01856-9.

4. Roukos, V., and Misteli, T. (2014). The biogenesis of chromosome translocations. Nat. Cell Biol. *16*, 293–300. 10.1038/ncb2941.

5. Ciccia, A., and Elledge, S.J. (2010). The DNA damage response: making it safe to play with knives. Mol. Cell *40*, 179–204. 10.1016/j.molcel.2010.09.019.

6. Scully, R., Panday, A., Elango, R., and Willis, N.A. (2019). DNA double-strand break repair-pathway choice in somatic mammalian cells. Nat. Rev. Mol. Cell Biol. *20*, 698–714. 10.1038/s41580-019-0152-0.

7. Hauer, M.H., and Gasser, S.M. (2017). Chromatin and nucleosome dynamics in DNA damage and repair. Genes Dev. *31*, 2204–2221. 10.1101/gad.307702.117.

8. Hoskins, R.A., Carlson, J.W., Kennedy, C., Acevedo, D., Evans-Holm, M., Frise, E., Wan, K.H., Park, S., Mendez-Lago, M., Rossi, F., et al. (2007). Sequence finishing and mapping of Drosophila melanogaster heterochromatin. Science *316*, 1625–1628. 10.1126/science.1139816.

9. Padeken, J., Zeller, P., and Gasser, S.M. (2015). Repeat DNA in genome organization and stability. Curr. Opin. Genet. Dev. *31*, 12–19. 10.1016/j.gde.2015.03.009.

10. Allshire, R.C., and Madhani, H.D. (2018). Ten principles of heterochromatin formation and function. Nat. Rev. Mol. Cell Biol. *19*, 229–244. 10.1038/nrm.2017.119.

11. Lachner, M., O'Carroll, D., Rea, S., Mechtler, K., and Jenuwein, T. (2001). Methylation of histone H3 lysine 9 creates a binding site for HP1 proteins. Nature *410*, 116–120. 10.1038/35065132.

12. Bannister, A.J., Zegerman, P., Partridge, J.F., Miska, E.A., Thomas, J.O., Allshire, R.C., and Kouzarides, T. (2001). Selective recognition of methylated lysine 9 on histone H3 by the HP1 chromo domain. Nature *410*, 120–124. 10.1038/35065138.

13. James, T.C., and Elgin, S.C. (1986). Identification of a nonhistone chromosomal protein associated with heterochromatin in Drosophila melanogaster and its gene. Mol. Cell. Biol. *6*, 3862–3872. 10.1128/mcb.6.11.3862-3872.1986.

14. Heitz, E. (1928). Das Heterochromatin der Moose. Jahrb Wiss Botanik *69*, 762–818.

15. Passarge, E. (1979). Emil Heitz and the concept of heterochromatin: longitudinal chromosome differentiation was recognized fifty years ago. Am. J. Hum. Genet. *31*, 106–115.

16. Strom, A.R., Emelyanov, A.V., Mir, M., Fyodorov, D.V., Darzacq, X., and Karpen, G.H. (2017). Phase separation drives heterochromatin domain formation. Nature *547*, 241–245. 10.1038/nature22989.

17. Larson, A.G., Elnatan, D., Keenen, M.M., Trnka, M.J., Johnston, J.B., Burlingame, A.L., Agard, D.A., Redding, S., and Narlikar, G.J. (2017). Liquid droplet formation by HP1α suggests a role for phase separation in heterochromatin. Nature *547*, 236–240. 10.1038/nature22822.

18. Chiolo, I., Minoda, A., Colmenares, S.U., Polyzos, A., Costes, S.V., and Karpen, G.H. (2011). Double-strand breaks in heterochromatin move outside of a dynamic HP1a domain to complete recombinational repair. Cell *144*, 732–744. 10.1016/j.cell.2011.02.012.

19. Ryu, T., Spatola, B., Delabaere, L., Bowlin, K., Hopp, H., Kunitake, R., Karpen, G.H., and Chiolo, I. (2015). Heterochromatic breaks move to the nuclear periphery to continue recombinational repair. Nat. Cell Biol. *17*, 1401–1411. 10.1038/ncb3258.

20. Janssen, A., Breuer, G.A., Brinkman, E.K., van der Meulen, A.I., Borden, S.V., van Steensel, B., Bindra, R.S., LaRocque, J.R., and Karpen, G.H. (2016). A single double-strand break system reveals repair dynamics and mechanisms in heterochromatin and euchromatin. Genes Dev. *30*, 1645–1657. 10.1101/gad.283028.116.

21. Tsouroula, K., Furst, A., Rogier, M., Heyer, V., Maglott-Roth, A., Ferrand, A., Reina-San-Martin, B., and Soutoglou, E. (2016). Temporal and Spatial Uncoupling of DNA Double Strand Break Repair Pathways within Mammalian Heterochromatin. Mol. Cell *63*, 293–305. 10.1016/j.molcel.2016.06.002.

22. Kendek, A., Wensveen, M.R., and Janssen, A. (2021). The Sound of Silence: How Silenced Chromatin Orchestrates the Repair of Double-Strand Breaks. Genes (Basel) *12*. 10.3390/genes12091415.

23. Ryu, T., Bonner, M.R., and Chiolo, I. (2016). Cervantes and Quijote protect heterochromatin from aberrant recombination and lead the way to the nuclear periphery. Nucleus *7*, 485–497. 10.1080/19491034.2016.1239683.

24. Uhlmann, F. (2016). SMC complexes: from DNA to chromosomes. Nat. Rev. Mol. Cell Biol. *17*, 399–412. 10.1038/nrm.2016.30.

25. Davidson, I.F., and Peters, J.-M. (2021). Genome folding through loop extrusion by SMC complexes. Nat. Rev. Mol. Cell Biol. *22*, 445–464. 10.1038/s41580-021-00349-7.

26. Pradhan, B., Kanno, T., Umeda Igarashi, M., Loke, M.S., Baaske, M.D., Wong, J.S.K., Jeppsson, K., Björkegren, C., and Kim, E. (2023). The Smc5/6 complex is a DNA loop-extruding motor. Nature *616*, 843–848. 10.1038/s41586-023-05963-3.

27. Jeppsson, K., Carlborg, K.K., Nakato, R., Berta, D.G., Lilienthal, I., Kanno, T., Lindqvist, A., Brink, M.C., Dantuma, N.P., Katou, Y., et al. (2014). The chromosomal association of the Smc5/6 complex depends on cohesion and predicts the level of sister chromatid entanglement. PLoS Genet. *10*, e1004680. 10.1371/journal.pgen.1004680.

28. Venegas, A.B., Natsume, T., Kanemaki, M., and Hickson, I.D. (2020). Inducible Degradation of the Human SMC5/6 Complex Reveals an Essential Role Only during Interphase. Cell Rep. *31*, 107533. 10.1016/j.celrep.2020.107533.

29. Potts, P.R., and Yu, H. (2007). The SMC5/6 complex maintains telomere length in ALT cancer cells through SUMOylation of telomere-binding proteins. Nat. Struct. Mol. Biol. *14*, 581–590. 10.1038/nsmb1259.

30. De Piccoli, G., Cortes-Ledesma, F., Ira, G., Torres-Rosell, J., Uhle, S., Farmer, S., Hwang, J.-Y., Machin, F., Ceschia, A., McAleenan, A., et al. (2006). Smc5-Smc6 mediate DNA double-strand-break repair by promoting sister-chromatid recombination. Nat. Cell Biol. *8*, 1032–1034. 10.1038/ncb1466.

31. Potts, P.R., Porteus, M.H., and Yu, H. (2006). Human SMC5/6 complex promotes sister chromatid homologous recombination by recruiting the SMC1/3 cohesin complex to double-strand breaks. EMBO J. *25*, 3377–3388. 10.1038/sj.emboj.7601218.

32. Mahrik, L., Stefanovie, B., Maresova, A., Princova, J., Kolesar, P., Lelkes, E., Faux, C., Helmlinger, D., Prevorovsky, M., and Palecek, J.J. (2023). The SAGA histone acetyltransferase module targets SMC5/6 to specific genes. Epigenetics Chromatin *16*, 6. 10.1186/s13072-023-00480-z.

33. Díaz, M., Pečinková, P., Nowicka, A., Baroux, C., Sakamoto, T., Gandha, P.Y., Jeřábková, H., Matsunaga, S., Grossniklaus, U., and Pecinka, A. (2019). The SMC5/6 complex subunit NSE4A is involved in DNA damage repair and seed development. Plant Cell *31*, 1579–1597. 10.1105/tpc.18.00043.

34. Clouaire, T., Rocher, V., Lashgari, A., Arnould, C., Aguirrebengoa, M., Biernacka, A., Skrzypczak, M., Aymard, F., Fongang, B., Dojer, N., et al. (2018). Comprehensive Mapping of Histone Modifications at DNA Double-Strand Breaks Deciphers Repair Pathway Chromatin Signatures. Mol. Cell *72*, 250-262.e6. 10.1016/j.molcel.2018.08.020.

35. Clouaire, T., and Legube, G. (2019). A Snapshot on the Cis Chromatin Response to DNA Double-Strand Breaks. Trends Genet. *35*, 330–345. 10.1016/j.tig.2019.02.003.

36. Colmenares, S.U., Swenson, J.M., Langley, S.A., Kennedy, C., Costes, S.V., and Karpen, G.H. (2017). Drosophila Histone Demethylase KDM4A Has Enzymatic and Non-enzymatic Roles in Controlling Heterochromatin Integrity. Dev. Cell *42*, 156-169.e5. 10.1016/j.devcel.2017.06.014.

37. Janssen, A., Colmenares, S.U., Lee, T., and Karpen, G.H. (2019). Timely double-strand break repair and pathway choice in pericentromeric heterochromatin depend on the histone demethylase dKDM4A. Genes Dev. *33*, 103–115. 10.1101/gad.317537.118.

38. Guo, R., Chen, J., Mitchell, D.L., and Johnson, D.G. (2011). GCN5 and E2F1 stimulate nucleotide excision repair by promoting H3K9 acetylation at sites of damage. Nucleic Acids Res. *39*, 1390–1397. 10.1093/nar/gkq983.

39. Tjeertes, J.V., Miller, K.M., and Jackson, S.P. (2009). Screen for DNA-damage-responsive histone modifications identifies H3K9Ac and H3K56Ac in human cells. EMBO J. *28*, 1878–1889. 10.1038/emboj.2009.119.

40. Lee, H.-S., Park, J.-H., Kim, S.-J., Kwon, S.-J., and Kwon, J. (2010). A cooperative activation loop among SWI/SNF, gamma-H2AX and H3 acetylation for DNA double-strand break repair. EMBO J. *29*, 1434–1445. 10.1038/emboj.2010.27.

41. Tamburini, B.A., and Tyler, J.K. (2005). Localized histone acetylation and deacetylation triggered by the homologous recombination pathway of double-strand DNA repair. Mol. Cell. Biol. *25*, 4903–4913. 10.1128/MCB.25.12.4903-4913.2005.

42. Feller, C., Forné, I., Imhof, A., and Becker, P.B. (2015). Global and specific responses of the histone acetylome to systematic perturbation. Mol. Cell *57*, 559–571. 10.1016/j.molcel.2014.12.008.

43. Karam, C.S., Kellner, W.A., Takenaka, N., Clemmons, A.W., and Corces, V.G. (2010). 14-3-3 mediates histone cross-talk during transcription elongation in Drosophila. PLoS Genet. *6*, e1000975. 10.1371/journal.pgen.1000975.

44. Carré, C., Szymczak, D., Pidoux, J., and Antoniewski, C. (2005). The histone H3 acetylase dGcn5 is a key player in Drosophila melanogaster metamorphosis. Mol. Cell. Biol. *25*, 8228–8238. 10.1128/MCB.25.18.8228-8238.2005.

45. Vamos, E.E., and Boros, I.M. (2012). The C-terminal domains of ADA2 proteins determine selective incorporation into GCN5-containing complexes that target histone H3 or H4 for acetylation. FEBS Lett. *586*, 3279–3286. 10.1016/j.febslet.2012.06.051.

46. Ciabrelli, F., Rabbani, L., Cardamone, F., Zenk, F., Löser, E., Schächtle, M.A., Mazina, M., Loubiere, V., and Iovino, N. (2023). CBP and Gcn5 drive zygotic genome activation independently of their catalytic activity. Sci. Adv. *9*, eadf2687. 10.1126/sciadv.adf2687.

47. Yu, D., Tan, Y., Chakraborty, M., Tomchik, S., and Davis, R.L. (2018). Elongator complex is required for long-term olfactory memory formation in Drosophila. Learn. Mem. *25*, 183–196. 10.1101/lm.046557.117.

48. Eissenberg, J.C., and Reuter, G. (2009). Chapter 1 Cellular Mechanism for Targeting Heterochromatin Formation in Drosophila. In International Review of Cell and Molecular Biology. (Elsevier), pp. 1–47. 10.1016/S1937-6448(08)01801-7.

49. Bennett, G., and Peterson, C.L. (2015). SWI/SNF recruitment to a DNA double-strand break by the NuA4 and Gcn5 histone acetyltransferases. DNA Repair (Amst) *30*, 38–45. 10.1016/j.dnarep.2015.03.006.

50. Zou, L., and Elledge, S.J. (2003). Sensing DNA damage through ATRIP recognition of RPA-ssDNA complexes. Science *300*, 1542–1548. 10.1126/science.1083430.

51. Ciurciu, A., Komonyi, O., Pankotai, T., and Boros, I.M. (2006). The Drosophila histone acetyltransferase Gcn5 and transcriptional adaptor Ada2a are involved in nucleosomal histone H4 acetylation. Mol. Cell. Biol. *26*, 9413–9423. 10.1128/MCB.01401-06.

52. Sancar, A., Lindsey-Boltz, L.A., Unsal-Kaçmaz, K., and Linn, S. (2004). Molecular mechanisms of mammalian DNA repair and the DNA damage checkpoints. Annu. Rev. Biochem. *73*, 39–85. 10.1146/annurev.biochem.73.011303.073723.

53. Laurençon, A., Purdy, A., Sekelsky, J., Hawley, R.S., and Su, T.T. (2003). Phenotypic analysis of separation-of-function alleles of MEI-41, Drosophila ATM/ATR. Genetics *164*, 589–601. 10.1093/genetics/164.2.589.

54. Brand, M., Moggs, J.G., Oulad-Abdelghani, M., Lejeune, F., Dilworth, F.J., Stevenin, J., Almouzni, G., and Tora, L. (2001). UV-damaged DNA-binding protein in the TFTC complex links DNA damage recognition to nucleosome acetylation. EMBO J. *20*, 3187–3196. 10.1093/emboj/20.12.3187.

55. Cheng, X., Côté, V., and Côté, J. (2021). NuA4 and SAGA acetyltransferase complexes cooperate for repair of DNA breaks by homologous recombination. PLoS Genet. *17*, e1009459. 10.1371/journal.pgen.1009459.

56. Dhalluin, C., Carlson, J.E., Zeng, L., He, C., Aggarwal, A.K., and Zhou, M.M. (1999). Structure and ligand of a histone acetyltransferase bromodomain. Nature *399*, 491–496. 10.1038/20974.

57. Miller, T.C.R., Simon, B., Rybin, V., Grötsch, H., Curtet, S., Khochbin, S., Carlomagno, T., and Müller, C.W. (2016). A bromodomain-DNA interaction facilitates acetylation-dependent bivalent nucleosome recognition by the BET protein BRDT. Nat. Commun. *7*, 13855. 10.1038/ncomms13855.

58. Filippakopoulos, P., Picaud, S., Mangos, M., Keates, T., Lambert, J.-P., Barsyte-Lovejoy, D., Felletar, I., Volkmer, R., Müller, S., Pawson, T., et al. (2012). Histone recognition and large-scale structural analysis of the human bromodomain family. Cell *149*, 214–231. 10.1016/j.cell.2012.02.013.

59. Marchand, J.-R., and Caflisch, A. (2015). Binding mode of acetylated histones to bromodomains: variations on a common motif. ChemMedChem *10*, 1327–1333. 10.1002/cmdc.201500141.

60. Pai, C.-C., Deegan, R.S., Subramanian, L., Gal, C., Sarkar, S., Blaikley, E.J., Walker, C., Hulme, L., Bernhard, E., Codlin, S., et al. (2014). A histone H3K36 chromatin switch coordinates DNA double-strand break repair pathway choice. Nat. Commun. *5*, 4091. 10.1038/ncomms5091.

61. Espinosa, M.C., Rehman, M.A., Chisamore-Robert, P., Jeffery, D., and Yankulov, K. (2010). GCN5 is a positive regulator of origins of DNA replication in Saccharomyces cerevisiae. PLoS ONE *5*, e8964. 10.1371/journal.pone.0008964.

62. Otterstrom, J., Castells-Garcia, A., Vicario, C., Gomez-Garcia, P.A., Cosma, M.P., and Lakadamyali, M. (2019). Super-resolution microscopy reveals how histone tail acetylation affects DNA compaction within nucleosomes in vivo. Nucleic Acids Res. *47*, 8470–8484. 10.1093/nar/gkz593.

63. Yin, H., Sweeney, S., Raha, D., Snyder, M., and Lin, H. (2011). A high-resolution whole-genome map of key chromatin modifications in the adult Drosophila melanogaster. PLoS Genet. *7*, e1002380. 10.1371/journal.pgen.1002380.

64. Xu, J., Ma, H., Jin, J., Uttam, S., Fu, R., Huang, Y., and Liu, Y. (2018). Super-Resolution Imaging of Higher-Order Chromatin Structures at Different Epigenomic States in Single Mammalian Cells. Cell Rep. *24*, 873–882. 10.1016/j.celrep.2018.06.085.

65. Gibson, B.A., Doolittle, L.K., Schneider, M.W.G., Jensen, L.E., Gamarra, N., Henry, L., Gerlich, D.W., Redding, S., and Rosen, M.K. (2019). Organization of chromatin by intrinsic and regulated phase separation. Cell *179*, 470-484.e21. 10.1016/j.cell.2019.08.037.

66. Clouaire, T., and Legube, G. (2015). DNA double strand break repair pathway choice: a chromatin based decision? Nucleus *6*, 107–113. 10.1080/19491034.2015.1010946.

67. Riddle, N.C., Minoda, A., Kharchenko, P.V., Alekseyenko, A.A., Schwartz, Y.B., Tolstorukov, M.Y., Gorchakov, A.A., Jaffe, J.D., Kennedy, C., Linder-Basso, D., et al. (2011). Plasticity in patterns of histone modifications and chromosomal proteins in Drosophila heterochromatin. Genome Res. *21*, 147–163. 10.1101/gr.110098.110.

68. O'Geen, H., Echipare, L., and Farnham, P.J. (2011). Using ChIP-seq technology to generate high-resolution profiles of histone modifications. Methods Mol. Biol. *791*, 265–286. 10.1007/978-1-61779-316-5_20.

69. Baymaz, H.I., Spruijt, C.G., and Vermeulen, M. (2014). Identifying nuclear protein-protein interactions using GFP affinity purification and SILAC-based quantitative mass spectrometry. Methods Mol. Biol. *1188*, 207–226. 10.1007/978-1-4939-1142-4_15.

Figure 1

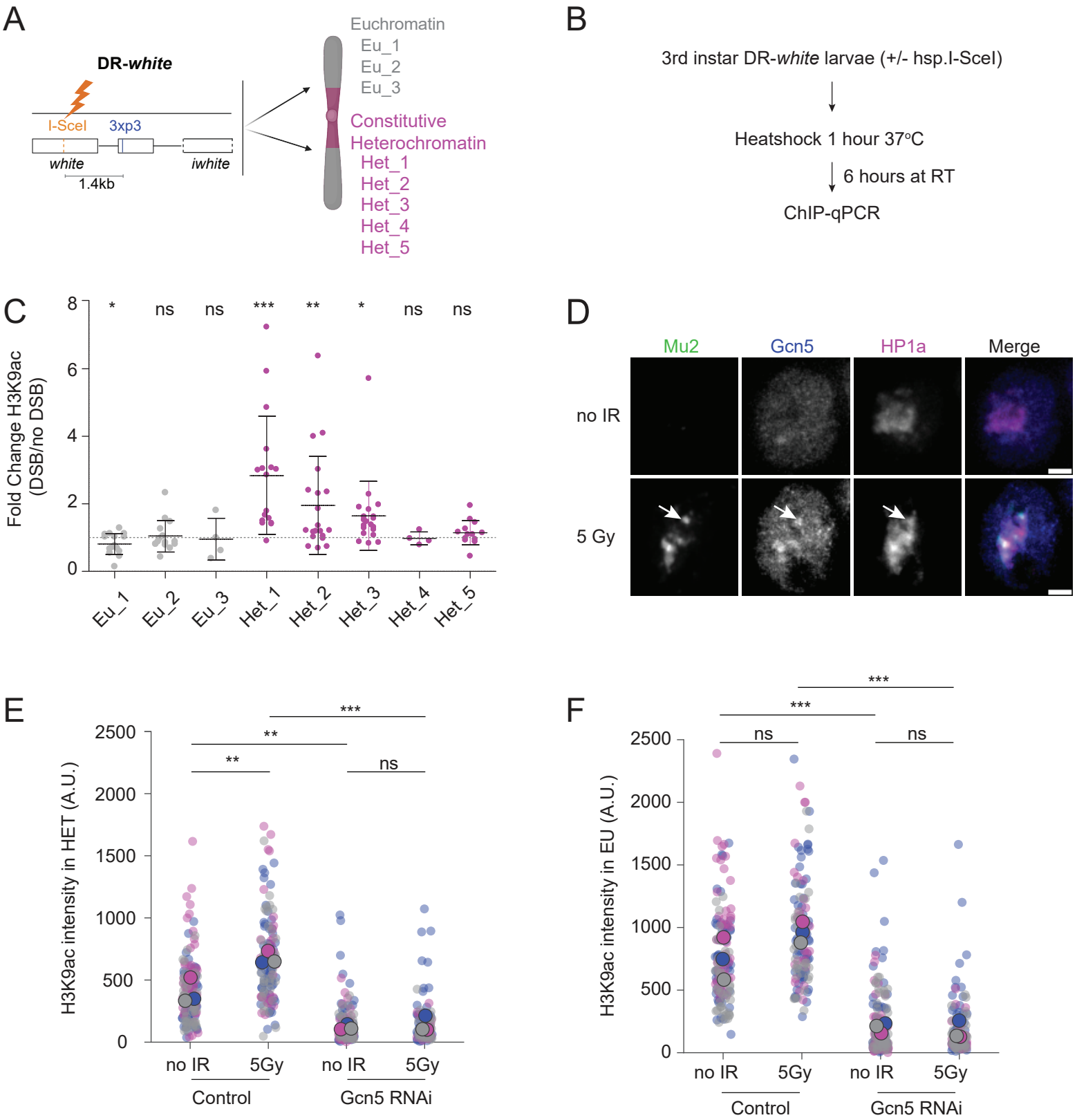
A
DR-white
I-SceI
3xp3
white
iwhite
1.4kb
Euchromatin
Eu_1
Eu_2
Eu_3
Constitutive
Heterochromatin
Het_1
Het_2
Het_3
Het_4
Het_5
B
3rd instar DR-white larvae (+/- hsp.I-SceI)
Heatshock 1 hour 37°C
6 hours at RT
ChIP-qPCR
C
Fold Change H3K9ac (DSB/no DSB)
* ns ns *** ** * ns ns
Eu_1 Eu_2 Eu_3 Het_1 Het_2 Het_3 Het_4 Het_5
D
Mu2
Gcn5
HP1a
Merge
no IR
5 Gy
E
H3K9ac intensity in HET (A.U.)
no IR 5Gy no IR 5Gy
Control
Gcn5 RNAi
F
H3K9ac intensity in EU (A.U.)
ns ns
no IR 5Gy no IR 5Gy
Control
Gcn5 RNAi

Figure 2

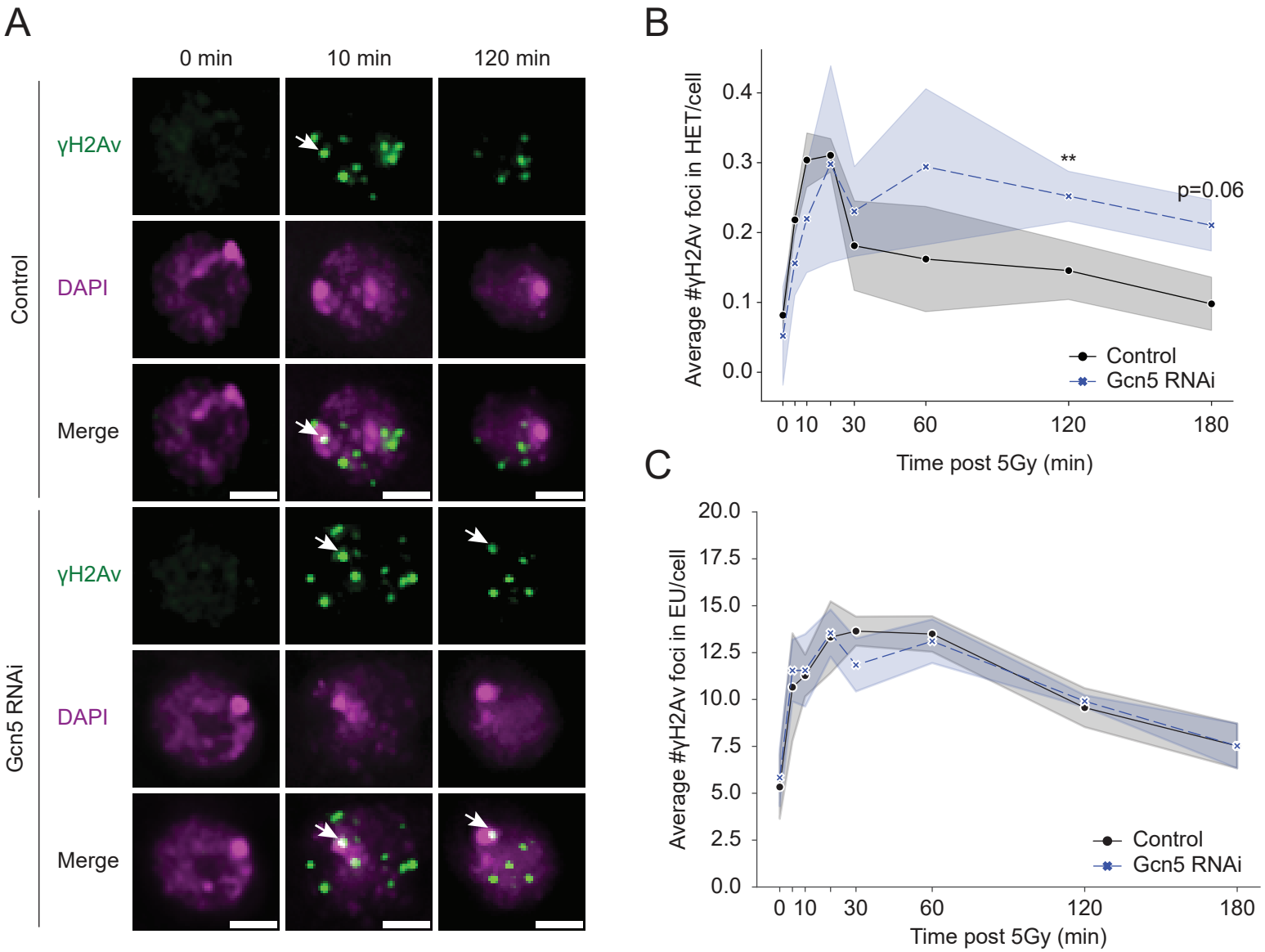
A
0 min
10 min
120 min
Control
γH2Av
DAPI
Merge
Gcn5 RNAi
γH2Av
DAPI
Merge
B
Average #γH2Av foci in HET/cell
0.4
0.3
0.2
0.1
0.0
**
p=0.06
Control
Gcn5 RNAi
0 10 30 60 120 180
Time post 5Gy (min)
C
Average #γH2Av foci in EU/cell
20.0
17.5
15.0
12.5
10.0
7.5
5.0
2.5
0.0
Control
Gcn5 RNAi
0 10 30 60 120 180
Time post 5Gy (min)

Figure 3

A

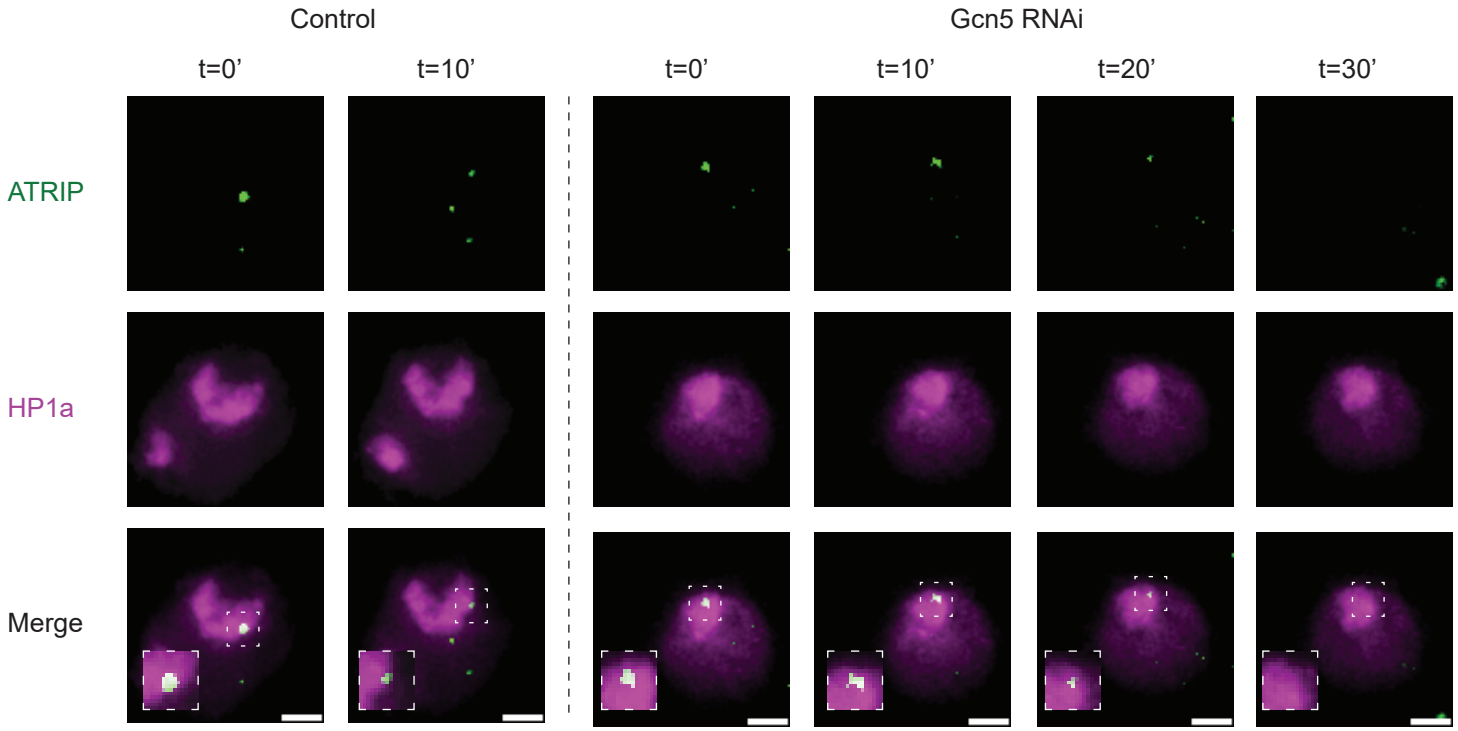
Control
Gcn5 RNAi
t=0'
t=10'
t=0'
t=10'
t=20'
t=30'
ATRIP
HP1a
Merge

B

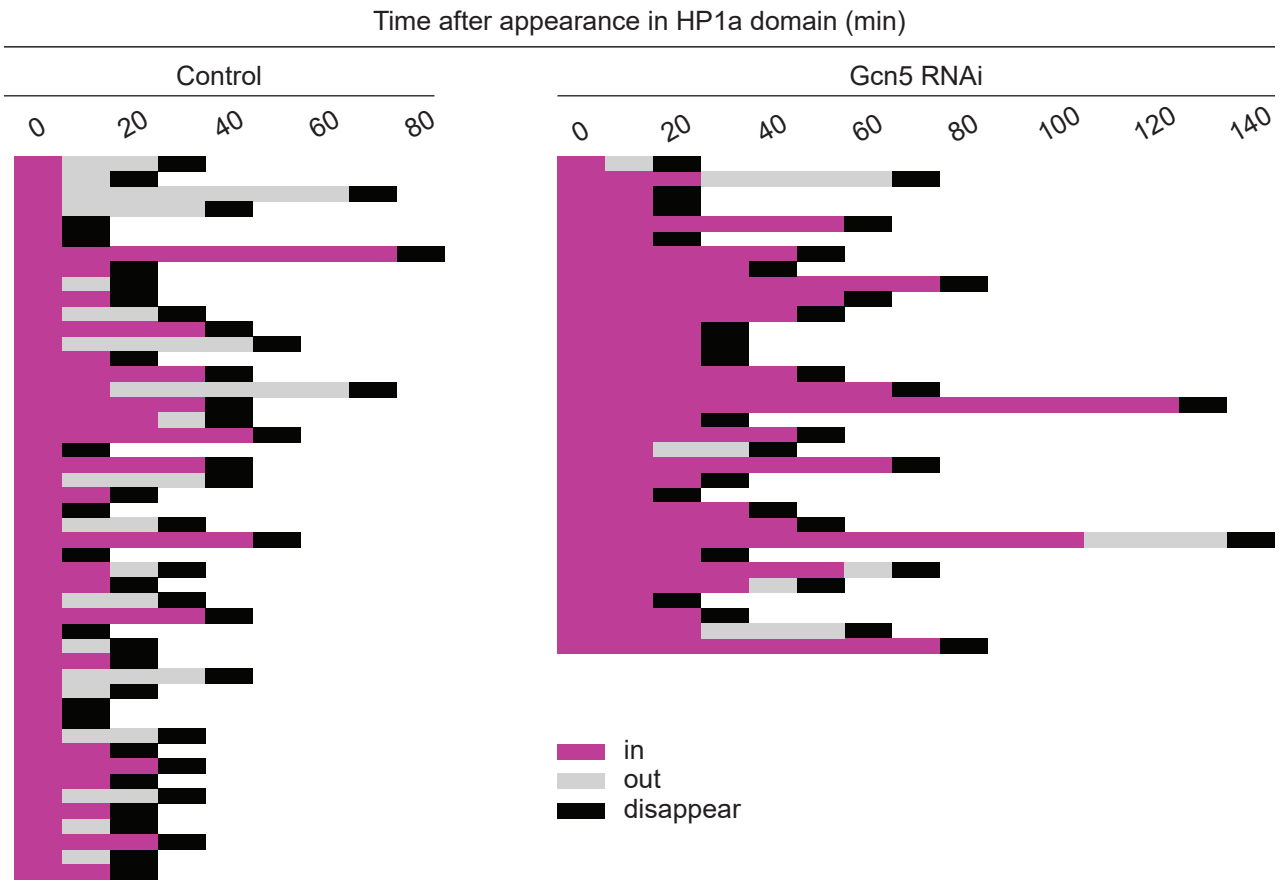
Time after appearance in HP1a domain (min)
Control
Gcn5 RNAi
0
20
40
60
80
0
20
40
60
80
100
120
140
in
out
disappear

C

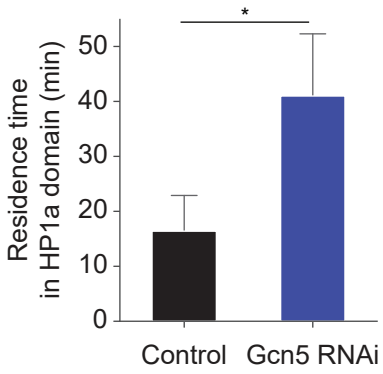
*
Residence time in HP1a domain (min)
50
40
30
20
10
0
Control
Gcn5 RNAi

Figure 4

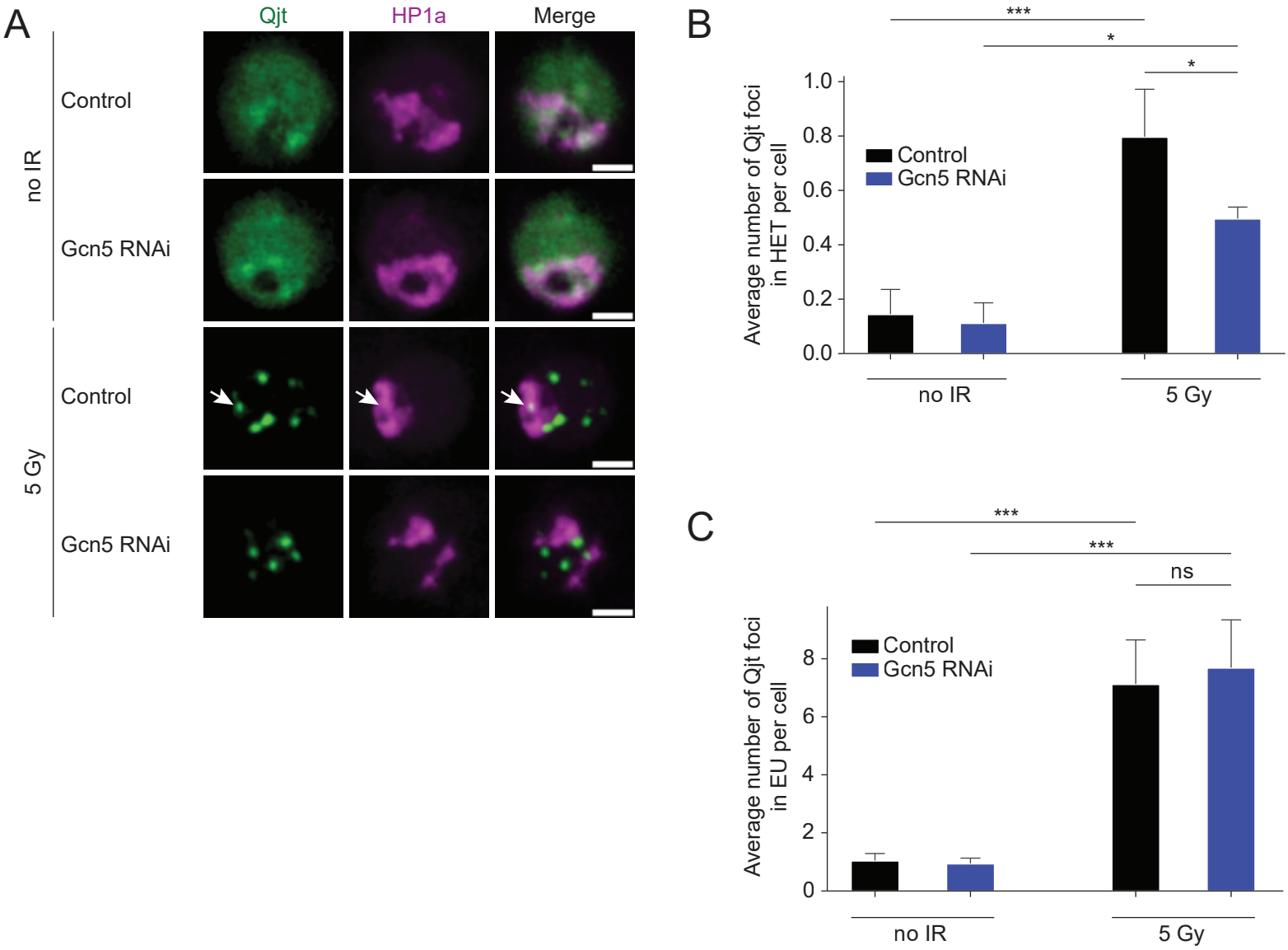
A
Qjt
HP1a
Merge
no IR
Control
Gcn5 RNAi
5 Gy
Control
Gcn5 RNAi
B
***
*
*
Average number of Qjt foci in HET per cell
1.0
0.8
0.6
0.4
0.2
0.0
Control
Gcn5 RNAi
no IR
5 Gy
C
***
***
ns
Average number of Qjt foci in EU per cell
8
6
4
2
0
Control
Gcn5 RNAi
no IR
5 Gy

Figure 5

A

C

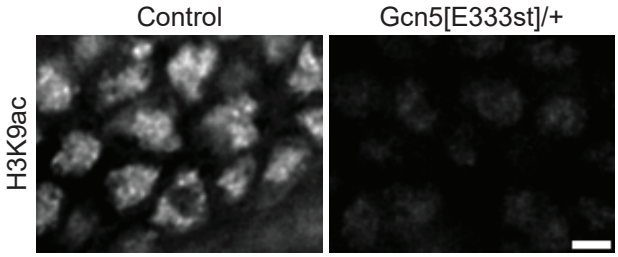

B

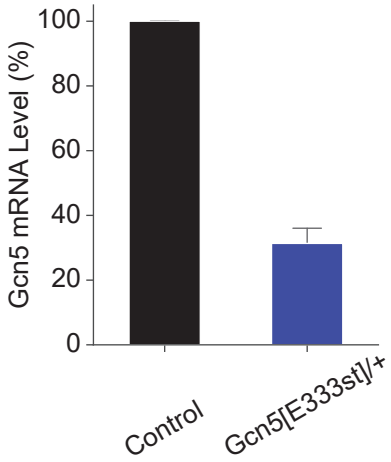

D

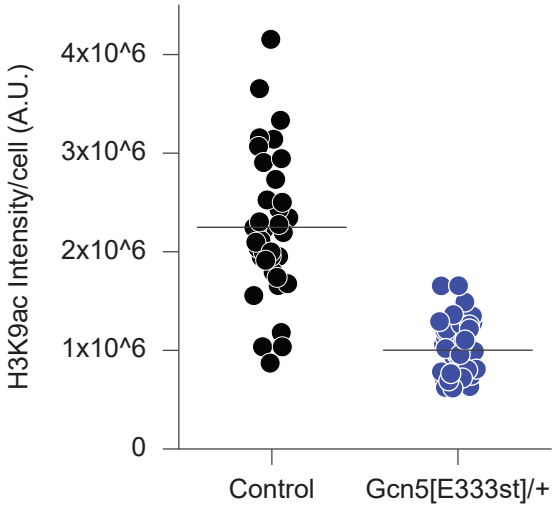

E

Genotype	Viability	N
Mei41+; Gcn5[E333st]/TM3	0.68767	310
Mei41[29D]; Gcn5[E333st]/TM3	0.48536	344
Relative viability of double mutant: 71% p-value 0.0004		

F

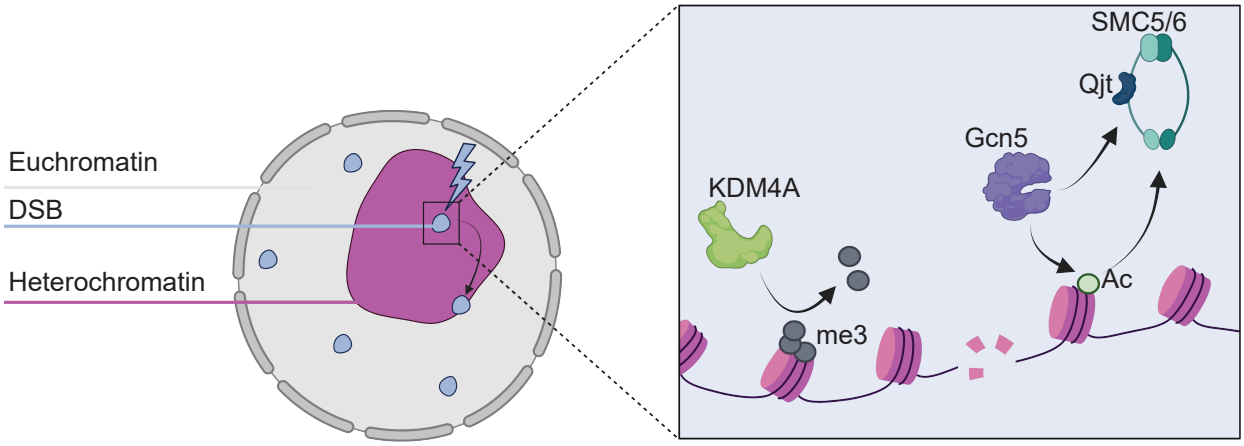

Figure S1

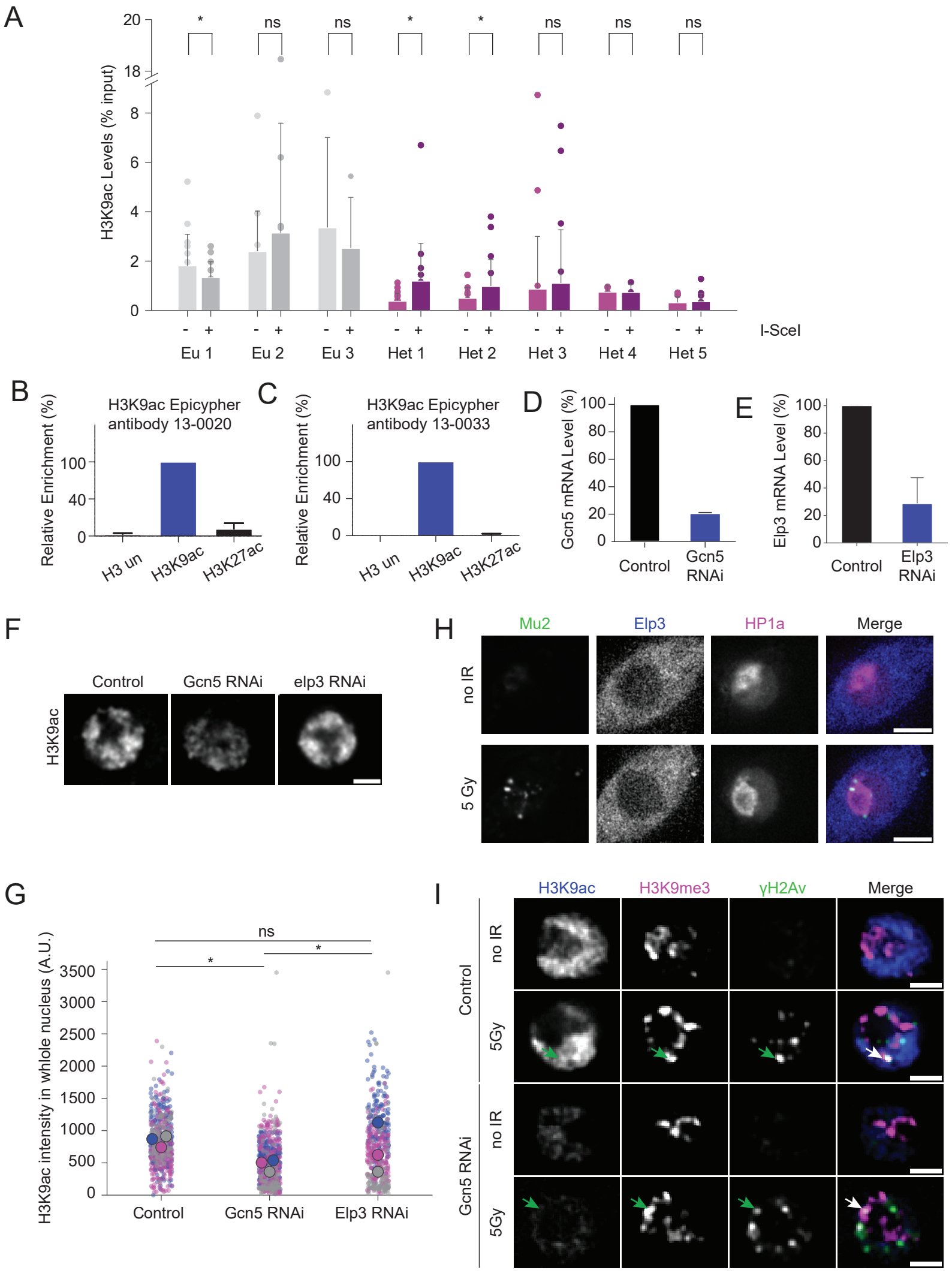
A
H3K9ac Levels (% input)
20
18
8
6
4
2
0
*
ns
ns
*
*
ns
ns
ns
- +
Eu 1
Eu 2
Eu 3
Het 1
Het 2
Het 3
Het 4
Het 5
I-SceI
B
H3K9ac Epicypher antibody 13-0020
Relative Enrichment (%)
100
40
0
H3 un
H3K9ac
H3K27ac
C
H3K9ac Epicypher antibody 13-0033
Relative Enrichment (%)
100
40
0
H3 un
H3K9ac
H3K27ac
D
Gcn5 mRNA Level (%)
100
80
60
40
20
0
Control
Gcn5 RNAi
E
Elp3 mRNA Level (%)
100
80
60
40
20
0
Control
Elp3 RNAi
F
Control
Gcn5 RNAi
elp3 RNAi
H3K9ac
H
Mu2
Elp3
HP1a
Merge
no IR
5 Gy
G
H3K9ac intensity in whole nucleus (A.U.)
3500
3000
2500
2000
1500
1000
500
0
ns
*
*
Control
Gcn5 RNAi
Elp3 RNAi
I
H3K9ac
H3K9me3
γH2Av
Merge
Control
no IR
5Gy
Gcn5 RNAi
no IR
5Gy

Figure S2

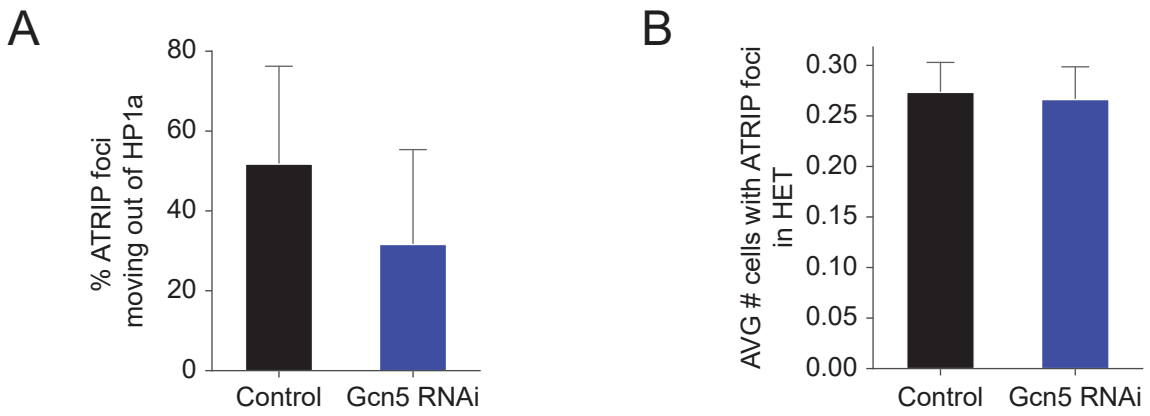
A
% ATRIP foci moving out of HP1a
80
60
40
20
0
Control
Gcn5 RNAi
B
AVG # cells with ATRIP foci in HET
0.30
0.25
0.20
0.15
0.10
0.05
0.00
Control
Gcn5 RNAi

Figure S3

A

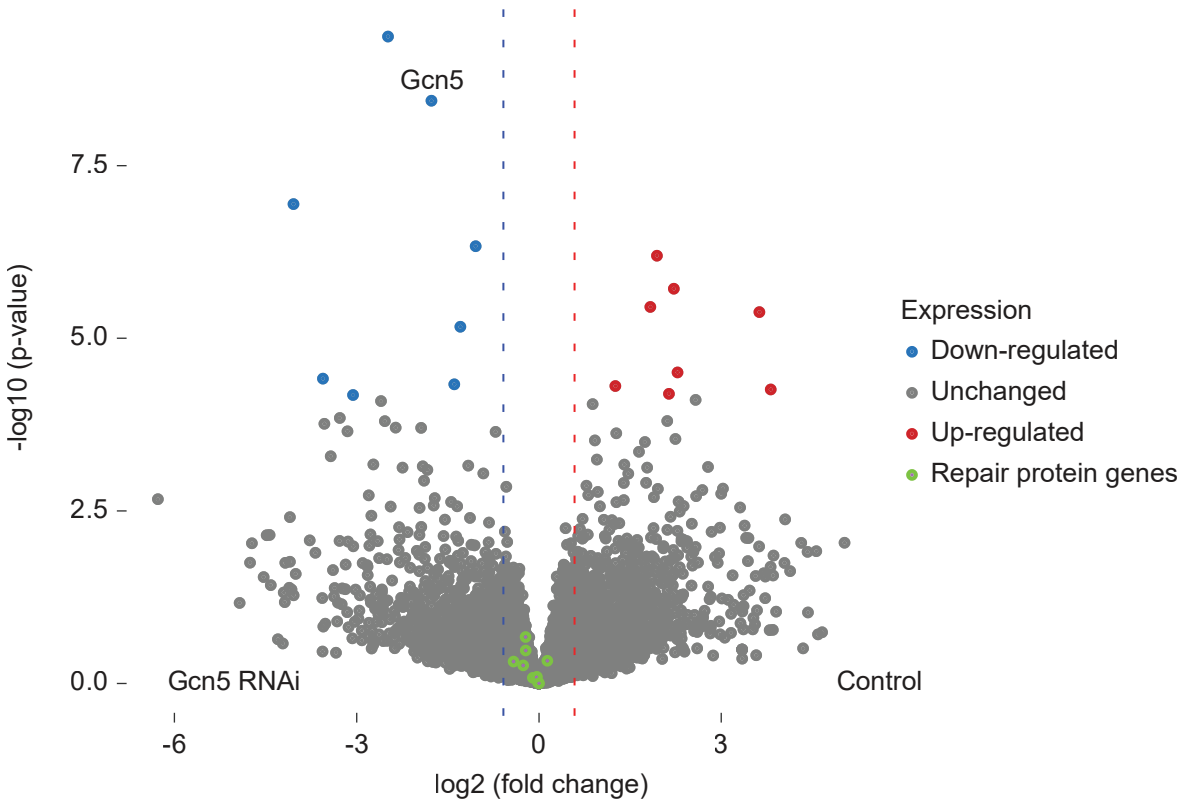
Gcn5
7.5
5.0
2.5
0.0
-log10 (p-value)
Gcn5 RNAi
Control
-6
-3
0
3
log2 (fold change)
Expression
Down-regulated
Unchanged
Up-regulated
Repair protein genes

B

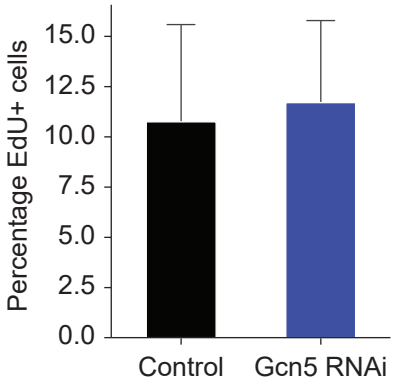
15.0
12.5
10.0
7.5
5.0
2.5
0.0
Percentage EdU+ cells
Control
Gcn5 RNAi

Figure S4

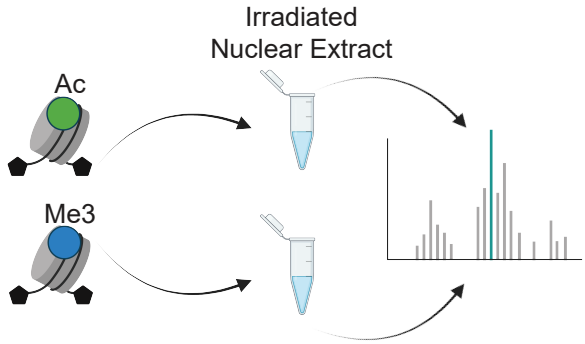
Irradiated
Nuclear Extract
Ac
Me3

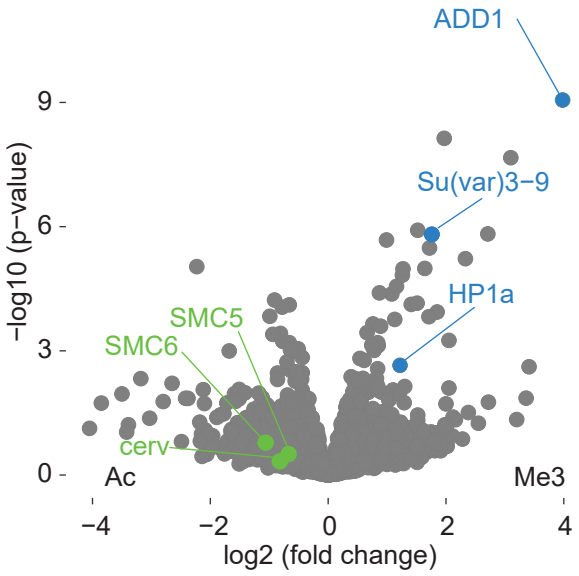
ADD1
Su(var)3−9
HP1a
SMC5
SMC6
cerv
Ac
Me3
−log10 (p−value)
9
6
3
0
−4
−2
0
2
4
log2 (fold change)